

**INVESTIGATION OF MICROBIAL BIOFILM
FORMATION USING ELECTROCHEMICAL
IMPEDANCE SPECTROSCOPY AND
EQUIVALENT CIRCUIT MODELLING**

**A Thesis Submitted to
the Graduate School of Engineering and Sciences of
İzmir Institute of Technology
in Partial Fulfillment of the Requirements for the Degree of**

**MASTER OF SCIENCE
in Materials Science and Engineering**

**by
Anılcan Kuş**

**July 2021
İZMİR**

ACKNOWLEDGMENTS

Firstly, I would like to thank Assist. Prof. Onur PARLAK for being a great mentor and a great mentor and scientific model. He believed in me when I lost my hope and directed me through this degree.

I want to thank my supervisor, Assoc. Prof. Dr Ümit Hakan YILDIZ with his suggestions and help with this thesis. Moreover, I would like to thank Prof. Dr Hasan ŞAHİN for giving me a chance to work in his lab in this pandemic.

Assoc. Prof. Dr Muhammed Üçüncü, Assoc. Prof. Aziz GENÇ, Assoc. Prof. Yaşar AKDOĞAN for their valuable comments and suggestions.

I thank Tuğrul Güner for his support and the answers he gave me through my master's. I want to also thank to my friends including Tuğçe Aybüke Arıca GÜVENÇ, Çetin Meriç GÜVENÇ, Yankı Öncü YAYAK, Mehmet BAŞKURT, Karen BUTINA, Hürriyet YÜCE, Mehmet BAŞKURT, Emre KARABURUN, Tuna DURAN, for their patience and support.

In this master's journey, being a guy dealing with ADHD and bipolar type II, I would like to say that the student's psychological situation and scientific skills should be considered. I learnt that mental health awareness should be mentioned much more frequently. After this achievement, I will discuss the mental health problems in academia, as I faced major depression and highly functioning anxiety to finish this thesis.

I wish to thank all of my family and psychiatrists for their supports. Therefore, I dedicate this thesis to academic depression and procrastinating.

ABSTRACT

INVESTIGATION OF MICROBIAL BIOFILM FORMATION USING ELECTROCHEMICAL IMPEDANCE SPECTROSCOPY AND EQUIVALENT CIRCUIT MODELLING

Bacterial biofilm is like a cooperative form of planktonic bacteria that colonize to acquire more nutritious and become resistant to surroundings. The communal organization results from the connection of bacteria by polysaccharides, lipids, or the extracellular matrix, which can provide a protective environment for living cells and communicate between them or allow specific types of chemicals inside through the matrix. 60%-80% of the infections are known to be biofilm-related. Bacterial biofilms are more resistant to antibiotics, and treating them with the wrong antibiotics might result in a thicker biofilm. In order to overcome these difficulties and researching new treatments for biofilm inflammation understanding the formation process is essential.

For this manner, Electrochemical Impedance Spectroscopy (EIS) has potential uses in various fields such as biosensors, corrosion studies, healthcare owing to its facile operation and affordable devices to conduct electroanalysis. EIS calculates the excitation voltage and current generated with the oscillating frequency. Developing impedimetric methods are gaining attention due to the operation being label-free. Considering its label-free nature, EIS is a possible candidate to explain the electrodynamics of living systems such as cell-matrix interaction, biofilm formation in vitro. Detection of those is essential to prevent infections and to develop medical needs to cure them. The thesis focuses on understanding the electrodynamics of bacterial biofilm formation via electrochemical methods such as square wave voltammetry (SWV), Open Circuit Potential (OCP), and EIS. After carrying out the experiments, time-dependent circuit models for EIS were built, and the data were extracted to demonstrate changes in the bacterial system.

ÖZET

MİKROBİYAL BİYOFİMLERİN ELEKTROKİMYASAL EMPEDANS SPEKTROSKOPİSİ VE EŞ DEVRE MODELLEMESİ İLE İNCELENMESİ

Mikrobiyal biyofilm, besinleri daha kolay elde etmek ve çevreye karşı dirençli hale gelmek için kolonileşen planktonik bakterilerin işbirlikçi bir formu gibidir. Komünal organizasyon, bakterilerin polisakkaritler, lipidler veya hücre dışı matris tarafından bağlanmasından kaynaklanır; bu, canlı hücreler için koruyucu bir ortam sağlayabilir ve bunlar arasında iletişim kurabilir veya matris yoluyla belirli kimyasal türlerinin içeri girmesine izin verebilir. Enfeksiyonların %60-80'inin biyofilm ile ilişkili olduğu bilinmektedir. Bakteriyel biyofilmler antibiyotiklere karşı daha dirençlidir ve bunları yanlış antibiyotiklerle tedavi etmek daha kalın bir biyofilm ile sonuçlanabilir. Bu zorlukların üstesinden gelmek ve biyofilm iltihabı için yeni tedaviler araştırmak için oluşum sürecini anlamak esastır.

Bu nedenle Elektrokimyasal Empedans Spektroskopisi (EIS), kolay çalışması ve elektroanaliz yapmak için uygun fiyatlı cihazları nedeniyle biyosensörler, korozyon çalışmaları, metal-organik çerçeveler ve en önemlisi sağlık gibi çeşitli alanlarda potansiyel kullanımlara sahiptir. EIS, salınım frekansı ile üretilen uyarma gerilimini ve akımı hesaplar. Operasyonun etiketsiz olması nedeniyle impedimetrik yöntemlerin geliştirilmesi dikkat çekmektedir. Etiketsiz doğası göz önüne alındığında, EIS, hücre-matris etkileşimi, in vitro biyofilm oluşumu gibi canlı sistemlerin elektrodinamiğini açıklamak için olası bir adaydır. Tez, kare dalga voltametri (SWV), Açık Devre Potansiyeli (OCP) ve EIS - gibi elektrokimyasal yöntemlerle bakteriyel biyofilm oluşumunun elektrodinamiğini anlamaya odaklanmaktadır. Deneyle gerçekleştirildikten sonra, EIS için zamana bağlı devre modelleri oluşturuldu ve bakteri sistemindeki değişiklikleri göstermek için veriler çıkarıldı.

Dedicated to academic depression and procrastinating...

TABLE OF CONTENTS

LIST OF FIGURES.....	viii
CHAPTER 1. INTRODUCTION.....	1
1.1. Motivation.....	1
1.2. The Structure and Scope of the Thesis	3
1.3. State of Art: Time-dependent Equivalent Circuit Modelling	3
CHAPTER 2. LITERATURE REVIEW.....	5
2.1. Biofilm.....	5
2.1.1. Detecting Pathogens	7
2.1.2. Polymerase Chain Reaction.....	9
2.1.3. Optotracing via Conjugated Oligothiophenes.....	10
2.2. Electrochemical Methods	12
2.2.1. Voltammetric Methods	12
2.2.2. Electrical Double-Layer.....	14
2.2.3. Electrochemical Impedance Spectroscopy	15
2.2.4. Equivalent Circuit Modelling	17
2.2.5. Applications of Electrochemical Impedance Spectroscopy.....	20
CHAPTER 3. EXPERIMENTAL.....	29
3.1. Methods	29
3.1.1. Bacterial strain and growth conditions	29
3.1.2. Electrochemical Measurements	29
3.1.3. Cleaning of Electrodes.....	30
3.1.4. Equivalent Circuit Modelling	30
3.1.5. Scanning Electron Microscopy and Sample Preparations	30
CHAPTER 4. RESULTS AND DISCUSSION.....	32
4.1. Experiments in Bulk Solution.....	32

4.1.1. Square Wave Voltammetry.....	34
4.1.2. Open Circuit Potential	36
4.1.3. Electrochemical Impedance Spectroscopy	37
4.2. Experiments at the Air-Liquid Interface.....	41
4.2.1. Square Wave Voltammetry.....	42
4.2.2. Open Circuit Potential	44
4.2.3. Electrochemical Impedance Spectroscopy	45
4.3. Scanning Electron Microscopy.....	48
CHAPTER 5. CONCLUSIONS	51
REFERENCES	52

LIST OF FIGURES

<u>Figure</u>	<u>Page</u>
Figure 1.1 Schematic illustration of the electrochemical impedance spectroscopy circuit models.....	3
Figure 2.1 Conceptualization of biofilm development and dynamic behaviours.....	6
Figure 2.2 Prevalence of health risks caused by microbial infections. (a) Foodborne pathogen caused hospitalizations in a year in the United States (b) From 2012 – 2014 Antibiotic-resistant UTI patients. (c) Projected number of deaths by cause in 2050 by antibiotic-resistant pathogens.	7
Figure 2.3 Schematic of biofilm formation and traditional detection methods.....	8
Figure 2.4 On the left: Aspect of staphylococcal colonies on Congo Red agar. (A) Red colonies of the non-slime-producing <i>Staphylococcus epidermidis</i> reference strain ATCC12228. (B) Black colonies of the slime-producing <i>S. epidermidis</i> reference strain RP62A. (C) Black colonies of <i>S. epidermidis</i> 709/85/bic/ep clinical isolate exhibited a red central zone at 48 hours, indicating the onset of a non-slime-producing phase variant. Right: PCR database	10

Figure 2.5 LCO-based morphotyping of *Salmonella* biofilms from agar plates. **(a)** Morphotypes of strain 3934 wt, $\Delta csgD$, $\Delta bcsA$ and $\Delta csgA$ based on the drop assay on Congo red plates. **(b)** Normalized spectra of h-FTAA mixed with re-suspended biofilm colonies harvested from indicated strains grown for 48 h on LB agar w/o salt, with emission read at 545 nm. h-FTAA mixed with cellulose and PBS were assayed in parallel for reference. **(c)** Morphotype of a 3934 wt biofilm colony originating from an individual bacterium on Congo red plates monitored for three consecutive days. **(d and e)** Spectra of h-FTAA mixed with harvested 3934 wt biofilm colonies at **(d)** days 2 and 3, and **(e)** day 1, including cellulose and PBS for reference. Arrows indicate the shift in λ_{max} for h-FTAA in the presence of various amounts of cellulose. *n*: 1 of 5 in **b** and **d**, *n*: 2 of 5 in **e**. Scale bars=1 cm. **(f)** Emission spectra of h-FTAA-supplemented cultures of strain 3934 wt, $\Delta bcsA$, $\Delta csgA$ and $\Delta csgD$ after 24 h incubation, using excitation at 405 nm for curli detection. **(g)** Same experimental setup as in **f** using excitation at 500 nm for cellulose detection. Arrows indicate λ_{max} of emission in $\Delta csgA$ and $\Delta csgD$ mutant strains. **(h)** Normalized fluorescence spectra for cellulose 11

Figure 2.6 **(A)** Cyclic voltammetry waveform, showing the initial potential (E_i) and the switching potential described by the maximum (E_f). **(B)** Cyclic voltammogram of a receptor-coated electrode **(a)** where its electrochemical response varies upon specific metabolite binding **(b)**. **(C)** Voltammetric profile of a bare electrode **(a)** and the electrochemical detection of bacterial metabolites **(b)**: based on their redox reaction on plain electrodes **(i)** or their enzyme-catalyzed conversion on specifically functionalized electrodes **(ii)**..... 13

<u>Figure</u>	<u>Page</u>
Figure 2.7 A) Potential–time profile of DPV. (B) Potential–time profile of SWV. (C) Representation of metabolite detection utilizing receptor coated electrodes: current variations are proportional to receptor occupancy. Initial potential (S1), the potential after the pulse (S2), pulse frequency (T) and pulse duration (tp).	14
Figure 2.8 Schematic drawing of Double Electrical Layer	15
Figure 2.9 Linear Immittance measuring setup	16
Figure 2.10 Plot describing the relationship between the input voltage, $E(t)$ and output current, $j(t)$ (or vice versa), the ratio of which results in impedance. ⁵³	17
Figure 2.11 General system characterization of electrochemical impedance spectroscopy.	18
Figure 2.12 Widely used equivalent circuit models for EIS fitting.	19
Figure 2.13 Admittance complex measurements carried out by Munoz et al. for <i>E. coli</i>	20
Figure 2.14 Concentration and Time Dependency of K_i	21
Figure 2.15 The equivalent circuit model to describe biofilm formation by EIS	22
Figure 2.16 Calculated a) capacitive b) resistive dynamics of <i>E. Coli</i> biofilm	23
Figure 2.17 Impedance analysis for the biofilms formation process. (A) Stages of biofilms formation process including reversible adhesion stage, irreversible adhesion stage, microcolony stage, mature stage and dispersal stage. (B) The equivalent circuit model for impedance analysis of Salmonella and <i>E. Coli</i> biofilms.	24
Figure 2.18 Fitting results of the equivalent circuit model for EIS of Salmonella and <i>E. Coli</i> biofilms as well as the results of Crystal violet staining experiments. (A) Trends of C_b during Salmonella biofilms formation process; (B) Trends of C_b during <i>E. Coli</i> biofilms formation process; (C) Trends of R_b during Salmonella biofilms formation process; (D) Trends of R_b during <i>E. Coli</i> biofilms formation process.	25

Figure 2.19 Impedance amplitude and phase spectrum of the three kinds of bacteria.
Bode impedance spectra of *S. mutans* (a), *A. viscosus* (c), and *L. fermentum* (e) on the Au, CE, and rGO-CE interface. Phase spectra of *S. mutans* (b), *A. viscosus* (d), and *L. fermentum* (f) on the Au, CE, and rGO-CE interface. 27

Figure 2.20 Statistical analysis of the impedance values of *S. mutans* (a), *A. viscosus* (b), and *L. fermentum* (c) attached to the surface of the different electrodes before and after biofilm formation. The data represent the mean of five results \pm standard deviation. The ΔZ of the three kinds of bacteria at different frequencies (d) 28

Figure 4.1. General Description of Experimental setup 32

Figure 4.2 Square Wave Voltammogram of the bulk experiments of three conditions. a) wild type strain b) mutant strain c) LB w/o salt 35

Figure 4.3 Open Circuit Potentials of the bulk experiments of three conditions. a) wild type strain b) mutant strain c) LB w/o salt 36

Figure 4.4 OCP Changes of three conditions 37

Figure 4.5 Equivalent Circuit Models for Impedance data fitting biofilm model is on the left, and bulk model is on the right 38

Figure 4.6 EIS experiments for wild type strain in bulk a) equivalent circuit model for EIS fitting b) Bode plot of EIS c) extracted charge transfer resistance d) extracted double-layer capacitance 39

Figure 4.7 EIS experiments for mutant strain in bulk a) equivalent circuit model for EIS fitting b) Bode plot of EIS c) extracted charge transfer resistance d) extracted double-layer capacitance 40

Figure 4.8 EIS experiments for LB w/o salt in bulk a) equivalent circuit model for EIS fitting b) Bode plot of EIS c) extracted charge transfer resistance d) extracted double-layer capacitance 41

Figure 4.9 Square Wave Voltammetry of wild type strain at the air-liquid interface 42

Figure 4.10 Square wave voltammetry for a) LB w/o salt b) mutant strain 43

<u>Figure</u>	<u>Page</u>
Figure 4.11 Open Circuit Potential measurements for three conditions in the air-liquid interface. a) wild type b) mutant strain c) LB w/o salt	44
Figure 4.12 OCP Changes of three conditions	45
Figure 4.13 EIS experiments for wild type strain in the air-liquid interface a) equivalent circuit model for EIS fitting after 24h b) Bode plot of EIS c) extracted charge transfer resistance d) extracted double-layer capacitance	45
Figure 4.14 Extracted C_{poly} and R_{poly} values according to added circuit elements.....	46
Figure 4.15 EIS experiments for mutant strain in the air-liquid interface a) equivalent circuit model for EIS fitting b) Bode plot of EIS c) extracted charge transfer resistance d) extracted double-layer capacitance	47
Figure 4.16 EIS experiments for LB w/o salt in the air-liquid interface a) equivalent circuit model for EIS fitting b) Bode plot of EIS c) extracted charge transfer resistance d) extracted double-layer capacitance.....	48
Figure 4.17 Schematics of Critical Point Drying Process (CPD).....	48
Figure 4.18 On the left Isolated biofilm after the experiment and on the right, re-dispersion in deionized water.....	49
Figure 4.19 Scanning electron microscopy analysis of regiospecific organizational states of Salmonella biofilms at the air-liquid interface	49
Figure 4.20 Scanning electron microscopy analysis of regiospecific organizational states of Salmonella biofilms at the air-liquid interface	50

CHAPTER 1

INTRODUCTION

1.1. Motivation

Preventing infection is a massive obstacle for humankind, as we see a viral infection causing a worldwide pandemic in 2020. Likewise, viral infection is a pandemic we are facing today; a bacterial pathogen causes a considerable number of infections, so the field of bacterial diagnostics is gaining significant attention. Before proceeding with the cure, first, detecting the pathogen as quickly as possible, developing non-destructive and fast-responding methods is crucial while fighting diseases since a patient's health is at risk. Different forms of bacteria can cause infections, such as planktonic growth, known as single-cell growth, or cellular aggregates as biofilms. Biofilms are like an adherent neighbourhood of bacteria that can adapt to different systems and gain various physical and chemical properties like antibiotic resistance.¹ Biofilm formation is a specific chain of events that begins with the attachment of bacteria to the surface. Then, cells produce an extracellular matrix (ECM) persisting of polymeric substances.²⁻⁴ Biofilm studies are an emerging field in healthcare, pollution and filtration of drinking water, and many biocatalytic processes such as biofuel cells and biochemical synthesis.⁵⁻⁹

Furthermore, they can be observed on both biotic and abiotic surfaces as known as solid surface-associated biofilms. Bacteria also grow in liquid conditions, either aerobic, dynamic or static conditions, and solid-surface-associated biofilm forms at the bottom container or sediment. This formation at the air-liquid interface is an excellent adaptation for bacteria since oxygen concentration is higher at the surface; bacteria can access oxygen effortlessly while still using the liquid medium's nutrition. On the other hand, biofilms are mentioned with different names such as pellicles, “floating” biofilm, or air-liquid interface biofilm.¹⁰⁻¹⁴ The microbiological approach of analyzing biofilms involves colourimetric assays of toxic dyes, biofilm-specific markers, and antibodies to detect. Unfortunately, these techniques disrupt the biofilm structure and composition due to removing the sample from its habitat analysis must be completed in an offline system, so gathering instant feedback on the biofilm structure and formation dynamics is

convoluted. These drawbacks are slowing down the understanding of the process, which is crucial since bacteria can be antibiotic-resistant with biofilm formation.¹⁵

Although biofilms' microbial properties are well characterized, electrodynamics, electrochemical features, and mechanical properties of formation at the air-liquid interface are currently not well experimented with electrochemical methods. Moreover, a requirement for labour might increase the cost. Hence, an approach that focuses on new cost, energy, and time-efficient methods is much needed to enlighten the shade. Several articles are present, which are described in the literature review section. However, these methods primarily focus on cell adhesion, biofouling or biosensing applications rather than specializing on biofilm itself, and proposed methodologies cannot differentiate regular cell adhesion from biofilm formation.

Electrochemical methods are a promising candidate for bacterial detection or in situ monitoring since they meet the increasing point-of-care era's expectations with personalized medicine in healthcare with cheaper manufacturing processes and time-efficient analysis. Main electrochemical methods are divided into subgroups depending on the analysis like potentiometric, colourimetric and impedimetric. Among the techniques, electrochemical impedance spectroscopy (EIS) is a simple method that calculates the current-voltage ratio of a system with changing frequencies of an excitation voltage. Moreover, with EIS, quantitative analysis can be achieved without labelling the strain, making it suitable for online monitoring of biofilm, and quantitative analysis can be carried out with equivalent circuit modelling.

In this thesis, *Salmonella Enteritidis* was used as a model system to study biofilm formation at the air-liquid interface with two different strains. A wild-type (wt) strain 3934 that can produce two principal components of biofilm, curli and cellulose, wt (cellulose+/curli+), and $\Delta csgD$ mutant of the same species that cannot form biofilm and cannot produce curli and cellulose, $\Delta csgD$ (cellulose-/curli-). By monitoring two different strains with distinct microbiological characteristics, the evolution of biofilm formation from single-cell to multicellular level by employing electrochemical impedance spectroscopy and potentiometric electrochemistry for quantitative electrochemical properties of the formation and redox dynamics of biofilm structure.

1.2. The Structure and Scope of the Thesis

The first chapter briefly introduces illness-causing bacteria, pathogens, biofilms while asking, “Why is a new method needed?”. In the 2nd chapter, a comprehensive review of Electrochemical Impedance Spectroscopy is carried out. In the 3rd chapter, experimental methods throughout thesis studies are given; the 4th chapter discusses the experiments' results using time-dependent impedance models and potentiometric electrochemical methods to support, and EIS 5th chapter concludes the study.

1.3. State of Art: Time-dependent Equivalent Circuit Modelling

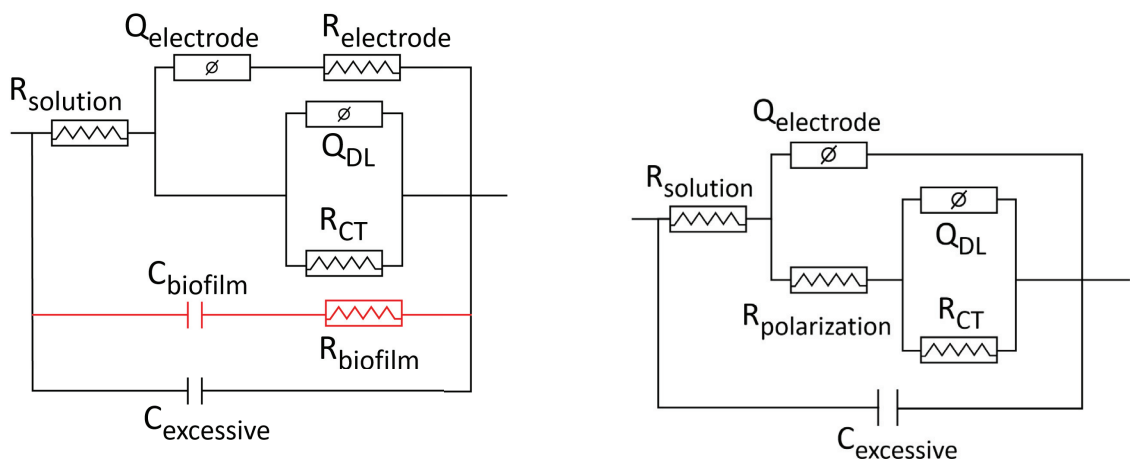


Figure 1.1 Schematic illustration of the electrochemical impedance spectroscopy circuit models

Two different equivalent circuit models were built, and the collected EIS data were fitted according to those models to illuminate biofilm formation and electrodynamics of extracellular components. The experiments were conducted in the air-liquid interface (interface) and in the solution (bulk) to distinguish biofilm's effect in the interface. In addition, bacteria samples were cultured on Luria-Bertani (LB w/o salt) without salt broth as a control experiment without bacteria; both interface and bulk experiments were conducted. Moreover, it is worth mentioning that the working electrode of the system was boron-doped-diamond (BDD) (with a surface area of 0.02 cm²). BDD is a durable electrode for extreme potentials and has a large scanning potential window,

little background signal, and low capacitive current. Electrode tubing was not used for direct analysis of biofilm formation in the interface.

Experiments were operated in this order, so growing dynamics, formation mechanism, and regio-temporal redox characteristics could be analyzed quantitatively.

- A strain with no biofilm $\Delta csgD$ (cellulose-/curli-)
- A biofilm-forming strain wt (cellulose+/curli+)

CHAPTER 2

LITERATURE REVIEW

2.1. Biofilm

The first mention of bacteria in the literature was by Antonie van Leeuwenhoek who analyzed bacteria on animal teeth. Then, the growth mechanism was thought to be floating single cells until Arthur T Henrici in the 1930s. He analyzed freshwater bacteria via microscopy and realized the bacterial community that grew on surfaces.¹⁶ The first article that came up with the “biofilm” analogy was published in 1961 by Rogovska et al. in *Microbiology-USSR*. After these findings, medical experts examined bacterial biofilms in the human body in 1973, and they observed *Pseudomonas aeruginosa* biofilms in the lungs.¹⁷ Costerton did the first illumination of biofilm formation in 1978, and he described biofilms in 1999 as “a structured community of bacterial cells enclosed in a self-produced polymeric matrix, adherent to a surface.”^{18,19}

Two types of bacterial growth are present: the free-living planktonic mode or structured communal growth as biofilms. Biofilms are attached to a surface growing as a group of bacteria sticking to each other or existing as a free-floating matrix kept by an extracellular matrix. Biofilm formation is a highly recognized mechanism of bacterial growth. The biofilm composition varies but mainly contains adhesins, amyloid-forming protein fibres, extracellular polysaccharides, and DNAs as ubiquitous components.

This colonization is based on “survival of the fittest”, and they stick together to survive more since bacteria can become resistant to their surroundings when biofilm forms. These communes are a reason for severe infections, as seen in plants or animals, including humans and medical devices and implants. Analyzing biofilms has an essential role in biotechnology in various fields such as cleaning wastewater, filtration of drinking water, biochemical synthesis or microbial fuel cells known as biocatalytic processes.

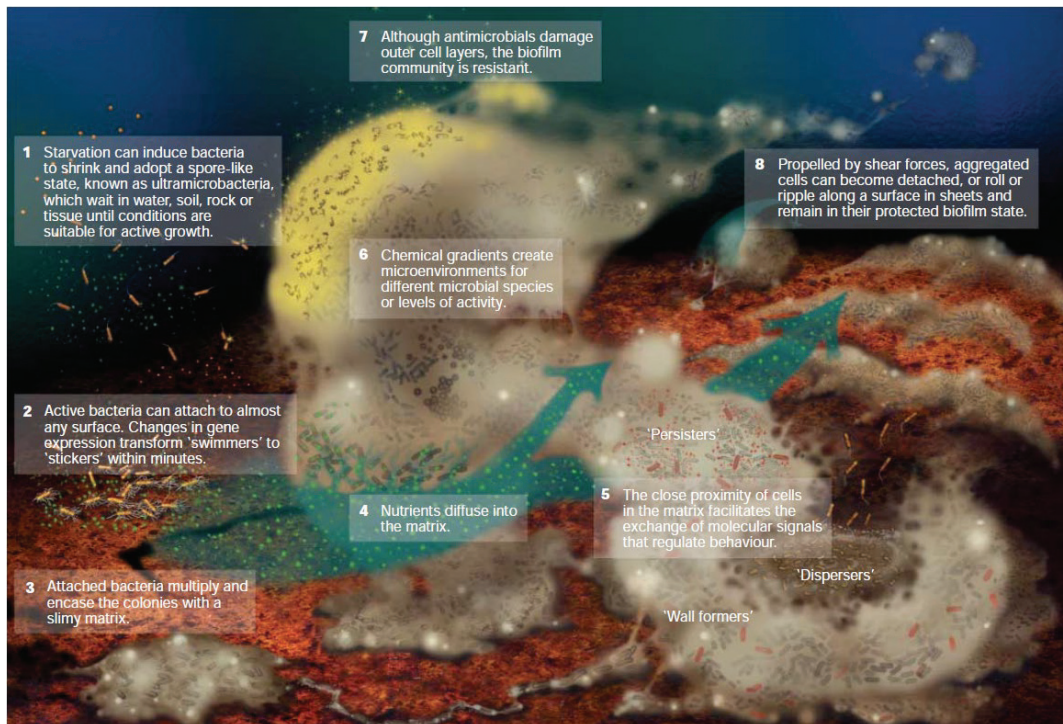


Figure 2.1 Conceptualization of biofilm development and dynamic behaviours.

(Source: *Nature Reviews Microbiology*. February 2004, pp 95–108).²⁰

Biofilms can build on nearly any biotic or abiotic surface and are sometimes known as stable floor-related biofilms. Bacteria also develop in a liquid beneath neath aerobic and static conditions, and they could both shape a stable surface-related biofilm at the lowest of the field or sediment. However, a few bacteria take advantage of the air-liquid interface to construct a floating community.^{3,4} This shape has generally termed the pellicle, 'floating' biofilm, or air-liquid interface biofilm. The biofilm formation on the air-liquid interface is a favourable ecological area of interest as it offers entry to excessive concentrations of oxygen originating from the air, similarly to the vitamin gift withinside the liquid.² Although microbiological factors of biofilm are well-studied, surprisingly, little is thought about their electrodynamics, interfacial electrochemical functions, and region-particular structural companies on the air-liquid interface shortage of interdisciplinary processes that permit direct size and evaluation of massive assemblies of densely packed cells.^{21–23}

2.1.1. Detecting Pathogens

Pathogens are one of the critical enemies of humankind for ailments due to the fact that they are able to multiply fast, and the biofilm can purpose antibiotic resistance. According to The Centers for Disease Control and Prevention (CDC), foodborne illnesses inflicting bacteria cause 50,000 and 1,500 hospitalized/dead human beings in a year, respectively.²⁴⁻²⁵ In addition to that, about 1,000,000 people are inflamed through Sexually Transferred bacterial illnesses (STI) each day that can purpose intense and persevering with health problems, from syphilis to congenital disabilities.²⁶ Moreover, a hundred and fifty million humans suffer from urinary tract infections (UTI), and a pair of million sufferers were hospitalized. As bacterial evolution persists thru increasing infections, a few instances can display antibiotic resistance; a pathogenic kind is broadly called gonorrhoea, quickly could be antibiotic-resistant.²⁷

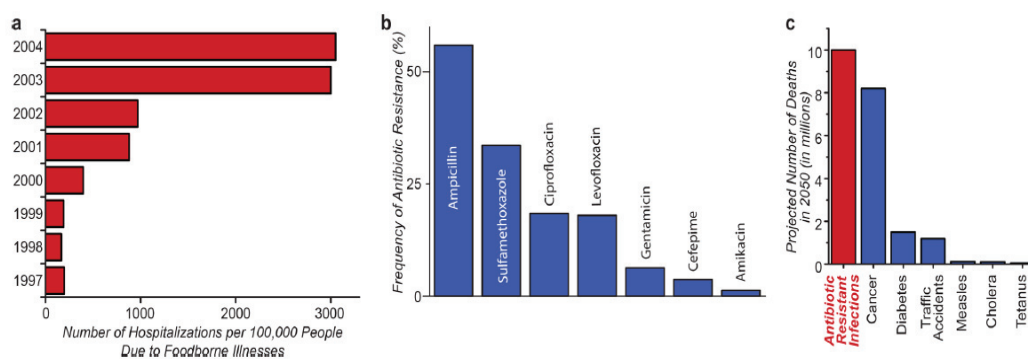


Figure 2.2 Prevalence of health risks caused by microbial infections. (a) Foodborne pathogen caused hospitalizations in a year in the United States (b) From 2012 – 2014 Antibiotic-resistant UTI patients. (c) Projected number of deaths by cause in 2050 by antibiotic-resistant pathogens.

(Source: Chem. Rev. 2019, 119 (1), 700–726.)²⁸

Figure 2.2 illuminates that developing quick methods to analyze pathogens is vital. Microbiological approaches to study biofilms eliminate the analyte from its environment, disrupting its local structure and composition and complicated microscopic or biochemical analyses. The present techniques stumble on, consisting of fluorescent dyes that restrict their use to end-factor sizes because of their toxicity.

They are offline and heavily depend on in-depth labour processes. They fail to immediately provide remarks on biofilm organization and different essential functions

and electrochemical and mechanical properties. Therefore, microbiologists cover strategies that can provide real-time statistics for the detection of biofilm.

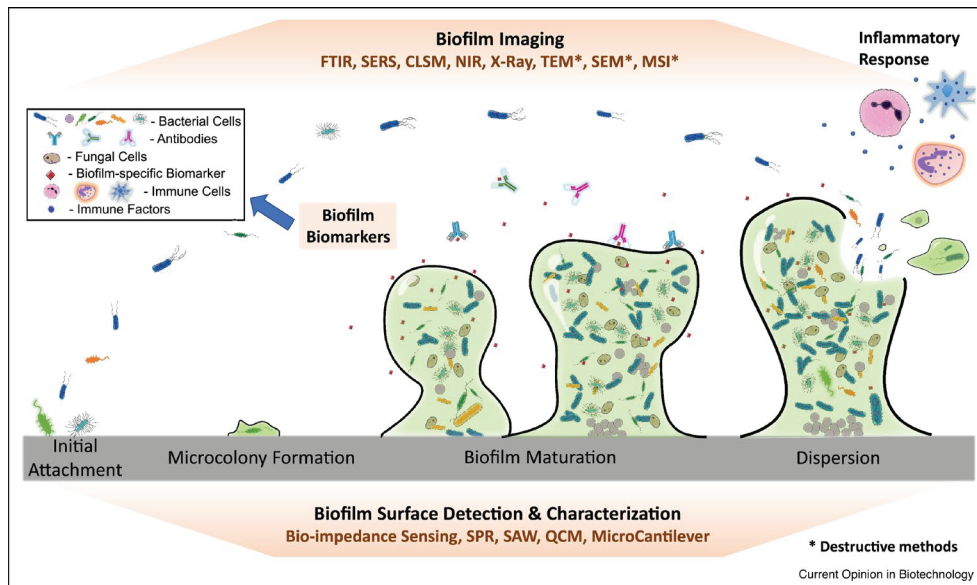


Figure 2.3 Schematic of biofilm formation and traditional detection methods

(Source: Current Opinion in Biotechnology. August 1, 2020, pp 79–84.)¹⁵

Figure 2.3 demonstrates the lack of suitable strategies for biofilm characterization. Although the analysis routines are achieved now, in clinical settings, they still have difficulties to solve.^{29–31} In general, infections due to biofilm stay in sites as seen in implant inflammations. With the clinical proof, it is known that the biofilm effect is unknown, or subclinical infections for more extended periods, the infection symptoms are less pronounced than acute infections, solely revealing themselves once biofilm cells shed off, leading to bacteriemia.³² Typically, infections with foreign bodies until device removal, even with the biofilm's removal characterization, require extensive processes to have proof. Once biofilm grows, the sampling becomes tougher on a device inside the body since surgery is necessary. This surgery primarily prohibits the detection of commonplace microbiological strategies akin to microorganisms culturing on agar plates until functioning access.

Notwithstanding the cells can be sampled, slow-growing bacteria might not form colonies beneath normal culturing conditions and might cause false adverse outcomes. The authors mentioned developing methods like SERS, HPLC, XPS in the last four years.¹⁵

2.1.2. Polymerase Chain Reaction

Polymerase Chain Reaction (PCR) is a method that provides amplification of one or many analytes' specific sequence of DNA; creating PCR based systems is very powerful since the amount of the analyte is relatively small with a fast and selective response. In fact, the PCR can sense one microorganism cell. PCR has been used to evaluate microorganism contamination in complex solutions. The literature suggests that finding different strains in a complicated water sample with small genetic information is possible.³³ Another benefit of PCR is specificity; specific bacteria can be sensed in different environments with a low detection limit. Although it is a fast and selective method, detecting multiple analytes requires additional work.

Moreover, this additional work brings multiplexed PCR, achieving that fast and selective method with multiple analytes. As mentioned by Kwon et al., analyzing various strains is possible with multiplexed PCR system. In addition to multiplexed PCR, Reverse Transcriptase Polymerase Chain Reaction (rt-PCR) is a different approach, and it focuses on RNA expression via complementary DNA (cDNA). It is valuable in detecting a single strain of a kind, but when it comes to analyzing biofilms, PCR development is pricy and hard to control.^{28,34-36}

Carla Renata Arciola et al. developed a method to observe biofilm formation mechanism by using a rapid detection method based on PCR for *S. epidermidis* and *S. aureus* by *icaA* and *icaD* genes. As they mention, *S. epidermidis* and *S. aureus* persist with *icaA* and *icaD* genes that help to produce extracellular polysaccharide slime. Congo Red agar was used as a control, and samples were taken from periprosthetic infections and healthy skin and mucosa. They proposed that the PCR method was reliable for slime-producing strains; thus, the biofilm-forming strains could be understood with PCR. Moreover, they presented an automatic sequence analyzing tool to determine the genes quickly.³³

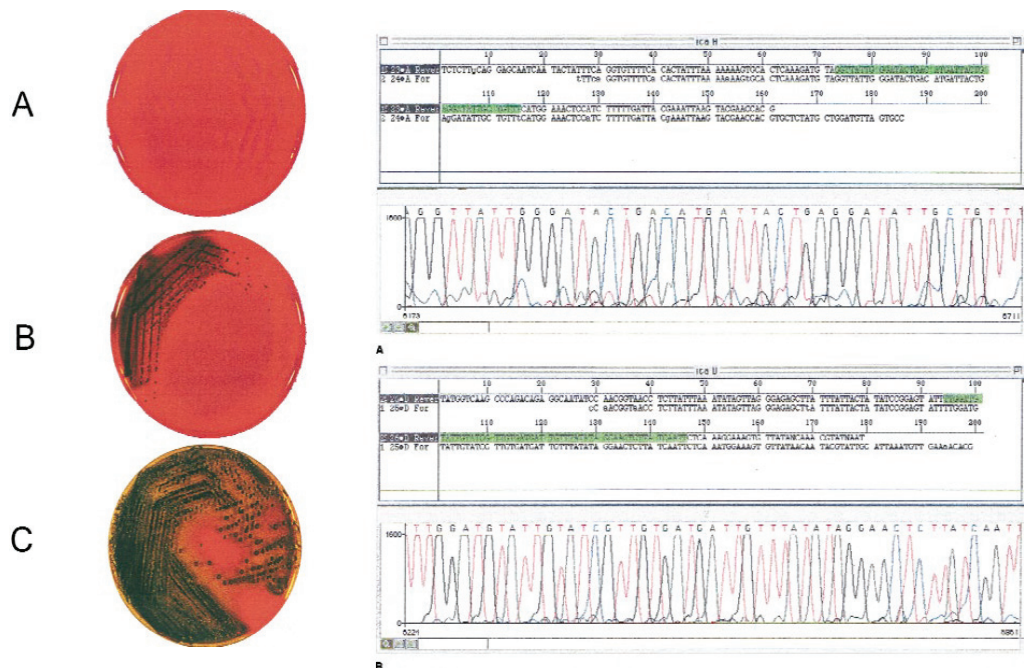


Figure 2.4 On the left: Aspect of staphylococcal colonies on Congo Red agar. (A) Red colonies of the non-slime-producing *Staphylococcus epidermidis* reference strain ATCC12228. (B) Black colonies of the slime-producing *S. epidermidis* reference strain RP62A. (C) Black colonies of *S. epidermidis* 709/85/bic/ep clinical isolate exhibited a red central zone at 48 hours, indicating the onset of a non-slime-producing phase variant. Right: PCR database

(Source: *Diagnostic Mol. Pathol.* **2001**, *10* (2), 130–137.)³³

2.1.3. Optotracing via Conjugated Oligothiophenes

It has been developed previously by several groups optotracers are conjugated oligothiophene (LCO) consisting of thiophene chains designed for the desired polymeric substances.^{37–39} The sensing mechanism of optotracers based on fluorescent type sensing. The absorbance/emission changes based on binding to the biorecognition element act as an ON/OFF type switch after binding to the polymeric substance of biofilms. Multivalent interactions of backbone and functional pendant groups in LCO. With these functionalized groups, detailed characterization like folding/unfolding of proteins can be carried out.^{40–42} Choong et al. proposed real-time monitoring of biofilm formation by using LCO based technology on *Salmonella* biofilm.⁴³

Curli and cellulose are biomolecular targets for optotracers; once they are bound to the bacterium, they have an emission analyzed by spectroscopic methods. One of the benefits of optotracers is it is non-toxic to bacterial strains; it can be used as an additional element in the matrix. The recordings showed that, via incubation of the microorganism,

optotracers showed unique peak emission for the specific component. Furthermore, this technique is incontestable for dynamic observation of biofilms since it is flexible and selective while the possibility to image biofilm formation in different mediums, even within the infected liver.

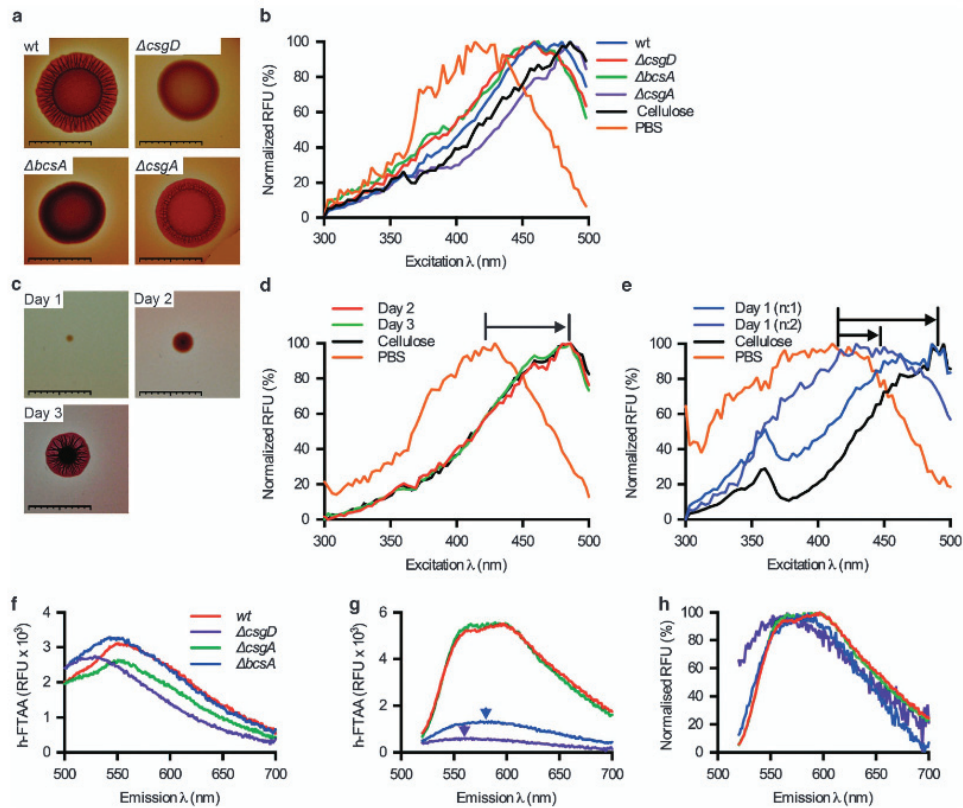


Figure 2.5 LCO-based morphotyping of *Salmonella* biofilms from agar plates. (a) Morphotypes of strain 3934 wt, $\Delta csgD$, $\Delta bcsA$ and $\Delta csgA$ based on the drop assay on Congo red plates. (b) Normalized spectra of h-FTAA mixed with re-suspended biofilm colonies harvested from indicated strains grown for 48 h on LB agar w/o salt, with emission read at 545 nm. h-FTAA mixed with cellulose and PBS were assayed in parallel for reference. (c) Morphotype of a 3934 wt biofilm colony originating from an individual bacterium on Congo red plates monitored for three consecutive days. (d and e) Spectra of h-FTAA mixed with harvested 3934 wt biofilm colonies at (d) days 2 and 3, and (e) day 1, including cellulose and PBS for reference. Arrows indicate the shift in λ_{max} for h-FTAA in the presence of various amounts of cellulose. n : 1 of 5 in b and d, n : 2 of 5 in e. Scale bars=1 cm. (f) Emission spectra of h-FTAA-supplemented cultures of strain 3934 wt, $\Delta bcsA$, $\Delta csgA$ and $\Delta csgD$ after 24 h incubation, using excitation at 405 nm for curli detection. (g) Same experimental setup as in f using excitation at 500 nm for cellulose detection. Arrows indicate λ_{max} of emission in $\Delta csgA$ and $\Delta csgD$ mutant strains. (h) Normalized fluorescence spectra for cellulose

(Source:npj Biofilms Microbiomes 2016, 2 (1), 1–11)⁴⁴

2.2. Electrochemical Methods

Electrochemical biosensors are rapidly growing in technology as we pursue the point-of-care era and personalized healthcare. Unlike the methods mentioned in Section 2.1.1, Electrochemical methods provide portable, easily handled, and cost-effective devices for detecting biofilms.⁴⁵ Several different electrochemistry approaches, such as voltammetric, amperometric/potentiometric, and impedimetric approaches. Herein, a brief discussion on the methods will be described.

2.2.1. Voltammetric Methods

One of the widely used methods in electrochemistry is voltammetry that analyzes voltage-dependent changes in current. The voltage swept enlightens oxidation/reduction potential, kinetics, and reaction mechanisms.⁴⁶ It has fundamentally two paths. The most common cyclic voltammetry (CV) is a method that spans between the desired upper and lower voltages linearly with a scan rate, which defines how fast the span is and the graph of CV drawn as Voltage vs Current. Two common ways exist to detect pathogens by a CV, as proposed in Figure 2.6B and 2.6C. The first way is using a receptor; when the analyte binds to the receptor, oxidation-reduction peaks shift and increase or decrease. The second option is performing oxidation-reduction with either a bare electrode or functionalizing the electrode for the desired analyte.

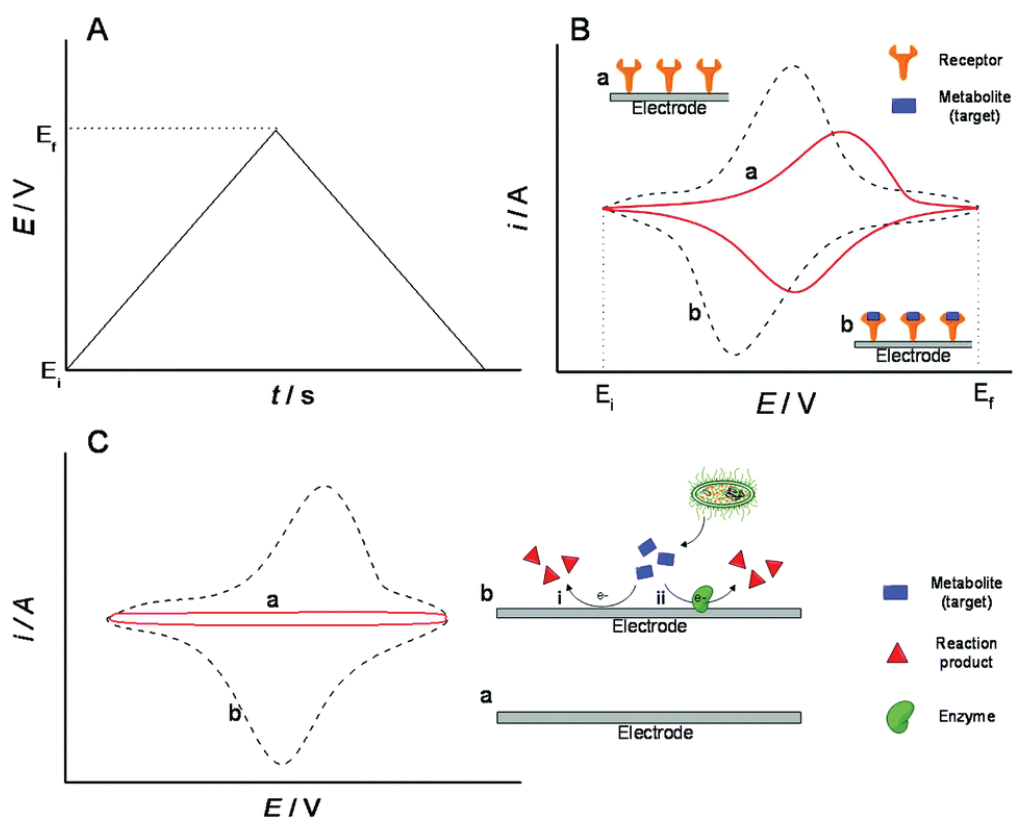


Figure 2.6 (A) Cyclic voltammetry waveform, showing the initial potential (E_i) and the switching potential described by the maximum (E_f). (B) Cyclic voltammogram of a receptor-coated electrode (a) where its electrochemical response varies upon specific metabolite binding (b). (C) Voltammetric profile of a bare electrode (a) and the electrochemical detection of bacterial metabolites (b): based on their redox reaction on plain electrodes (i) or their enzyme-catalyzed conversion on specifically functionalized electrodes (ii).

(Source: Fundamentals, Achievements and Challenges in the Electrochemical Sensing of Pathogens. *Analyst*. Royal Society of Chemistry November 7, 2015, pp 7116–7128.)⁴⁶

Along with cyclic voltammetry, pulse voltammetry is a widely used method that provides lower detection limits and eliminates capacitive currents via applying ladder-like voltages. Differential Pulse Voltammetry (DPV) voltage is scanned through constant growth in every step; SWV mainly involves applying a series of potential pulses formed from a potential staircase overlaid with a square wave pulse a forward and then reverse pulse occurring on each tread of the staircase. While working on higher frequencies, the capacitive current is eliminated in pulse voltammetry due to a rapid decrease in charging current than faradaic current; it is why the detection limit is much smaller in pulse

voltammetry. Also, square wave voltammetry is faster than any other with avoiding oxygen peaks generated among these methods.

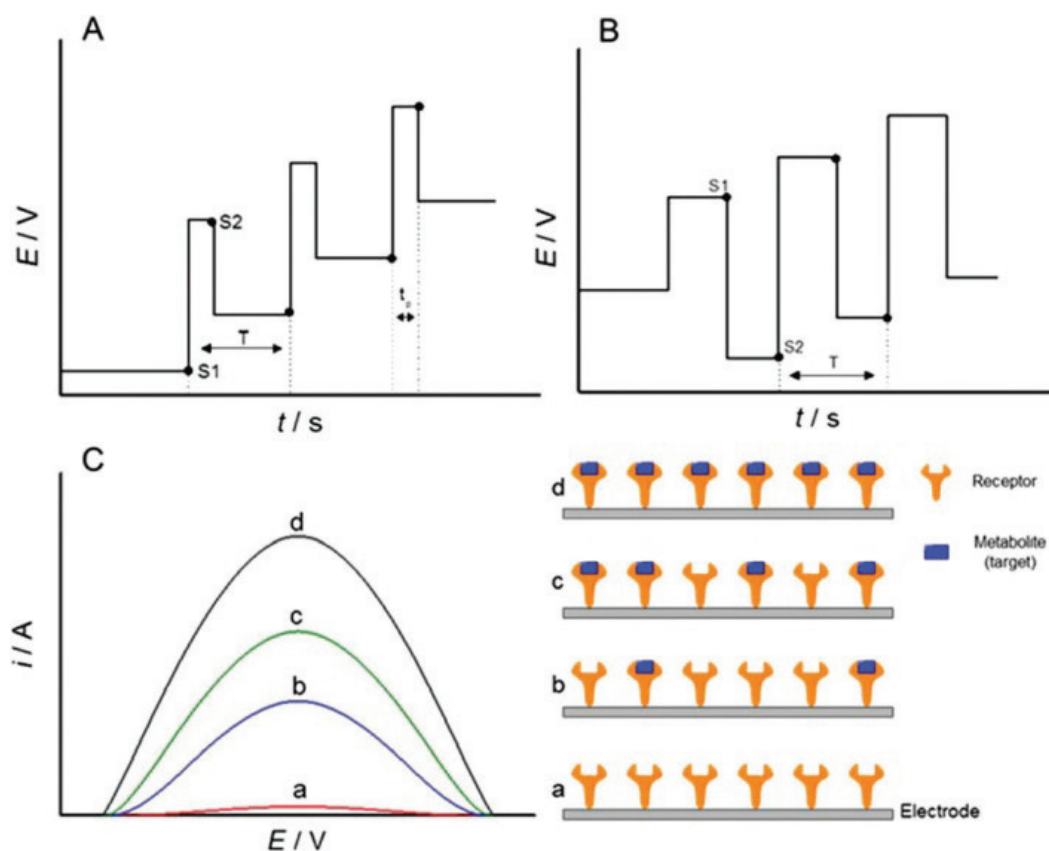


Figure 2.7 A) Potential–time profile of DPV. (B) Potential–time profile of SWV. (C) Representation of metabolite detection utilizing receptor coated electrodes: current variations are proportional to receptor occupancy. Initial potential (S1), the potential after the pulse (S2), pulse frequency (T) and pulse duration (t_p).

(Source: Fundamentals, Achievements and Challenges in the Electrochemical Sensing of Pathogens. *Analyst*. Royal Society of Chemistry November 7, 2015, pp 7116–7128.)⁴⁶

2.2.2. Electrical Double-Layer

One of the pioneers of electrochemistry, von Helmholtz, demonstrated that even without electrochemical reactions, the metal/electrolyte persists the interface, and he named that interface as Electrical Double Layer (DL).⁴⁵ This observed interface is acting as a capacitor and exists in the whole electrochemical system. After Helmholtz, Cole and Chapman developed his theory with experiments and mathematics in 1910 and 1915.⁴⁷⁻⁴⁸ The DL fundamentally describes how charged or polarized systems will behave with an applied voltage to the electrode, as shown in Figure 2.8.

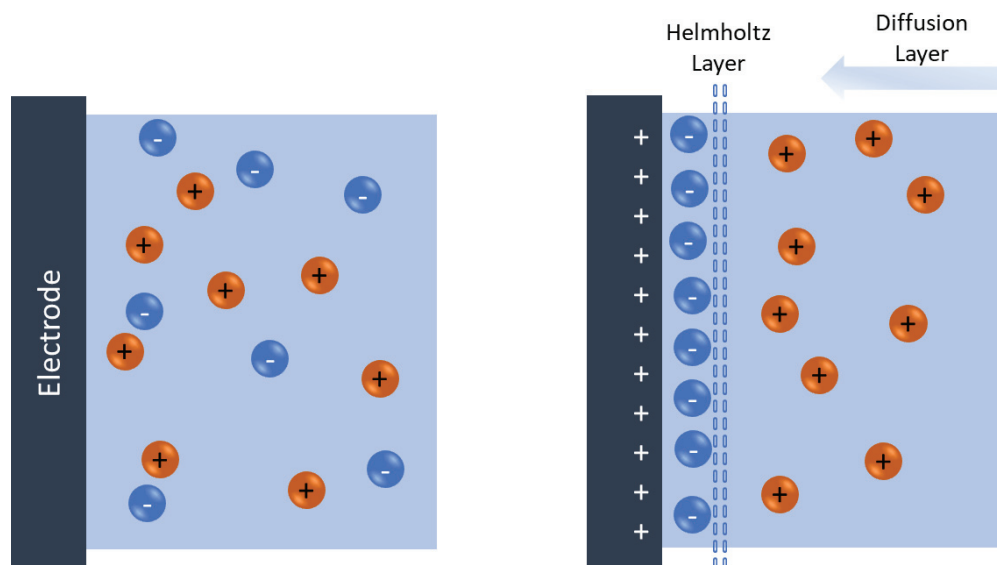


Figure 2.8 Schematic drawing of Double Electrical Layer

2.2.3. Electrochemical Impedance Spectroscopy

Electrochemical Impedance Spectroscopy (EIS) is a robust method requiring little to no labelling; rapid and non-destructive methods become a promising tool. Even if it is a simple method theoretically with the current developments in EIS, it can be found in numerous fields such as the characterization of energy sources, planet surface analysis, semiconductors, and most importantly, in healthcare. Oliver Heaviside carried out the first records of EIS in the literature in 1886. After Heaviside in 1928, Kenneth Cole and Howard carried out the first living cell experiments.⁴⁹⁻⁵¹ Years after, Keese and Giaever started using this label-free approach; they developed microelectronics to Wegener, J.; Keese analyzed cell-substrate analysis.⁵²

The impedance is a complex matrix that depends on a frequency of excitation, voltage, can be shown as Z or $Z(\omega)$. As impedance refers to a voltage, admittance, which is a complex conductivity, persists along with the impedance and denoted as '1/ Z ' or 'Y'.

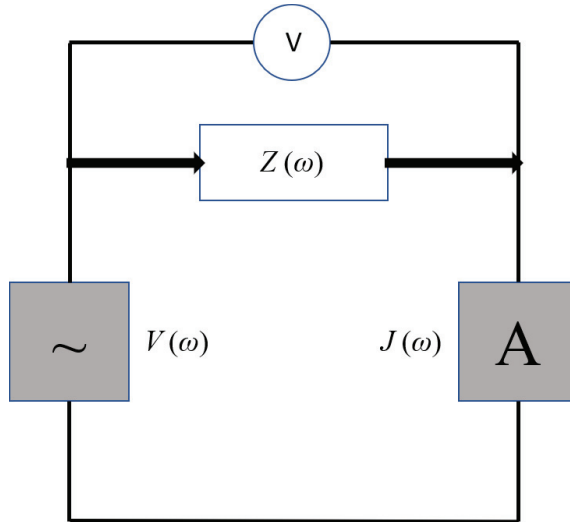


Figure 2.9 Linear Immittance measuring setup

As complex identities should be, impedance and admittance have real and imaginary parts, and by using mathematics, impedance analysis becomes a valuable tool to clarify the characteristics of the system. In literature, the impedance or admittance functions are called “immittance” as a global term. These functions are sinusoidal in a single-frequency region if a sample is a linear one. The excitation voltage a time-dependent quantity shown in equation-X, and the current response of that voltage sinusoidal in equation-Y. Herein, “ J ” is the current response, and “ φ ” a substantial quantity corresponds to phase shift due to excitation voltage. Therefore, the impedance that is based on Ohm’s Law will be equation-Z.

$$V(\omega) = V_0 e^{i\omega t} \quad (1)$$

$$J(\omega) = J_0 e^{i\omega t} \cdot e^{i\varphi} \quad (2)$$

$$Z(\omega) = \frac{V(\omega)}{J(\omega)} = \frac{V_0}{J_0} e^{i\varphi} = |Z| e^{i\varphi} = Z' + iZ'' \quad (3)$$

Figure 2.9 shows the basic immittance measurement setup in theory. The linearity that was mentioned means that the excitation voltage applied should relate to the current observed. Equation 1 is time-dependent with frequency dependency, the excitation voltage’s harmonics can be expressed as a summation of $V(\omega)$ ’s shown in equation-2. Since the immittance is linear, the admittance or current can also be calculated with integration in equation 3. Moreover, EIS can be used for non-linear systems such as

semiconductors by applying a large voltage to overcome the bandgap with a small-oscillating excitation voltage.

$$V(t) = \int_{-\infty}^{\infty} \tilde{V}(\omega) e^{i\omega t} d\omega \quad (4)$$

$$J(t) = - \int_{-\infty}^{\infty} \frac{\tilde{v}(\omega)}{\tilde{z}(\omega)} e^{i\omega t} d\omega = - \int_{-\infty}^{\infty} Y(\omega) \tilde{V}(\omega) e^{i\omega t} d\omega \quad (5)$$

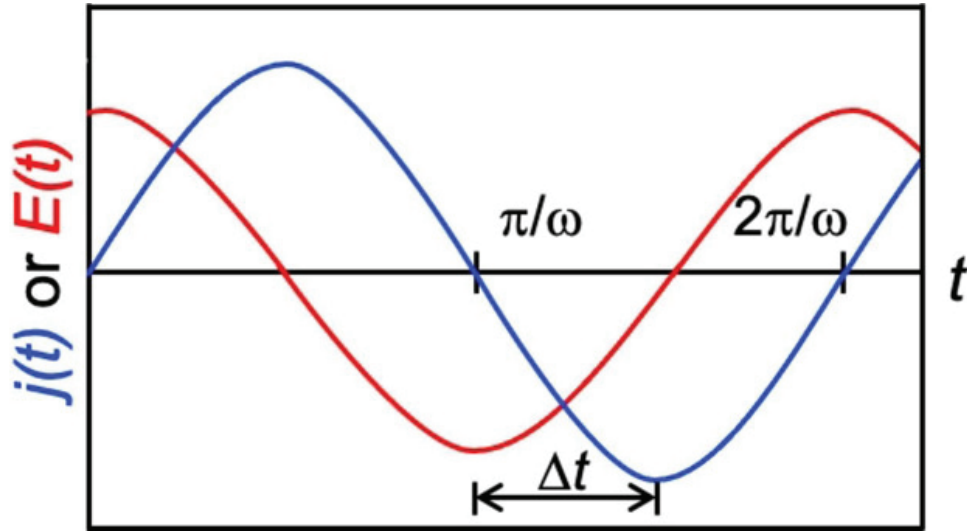


Figure 2.10 Plot describing the relationship between the input voltage, $E(t)$ and output current, $j(t)$ (or vice versa), the ratio of which results in impedance.⁵³

2.2.4. Equivalent Circuit Modelling

Equivalent circuit models are mathematical expressions that correspond to a circuit model built based on the experiments. With the help of models, extracting the data from the graph becomes viable, and it lightens the characteristics of the sample. A diagram that explains the fundamentals of data analysis of EIS is shown in Figure 2.10. As mentioned in the diagram, there are two basic ways to extract EIS data, either with exact mathematical expression or the equivalent circuit model that corresponds to that mathematical expression.⁵⁴ The second way is easier since the modern software made it user friendly by adding elements on paper without dealing with the math. Also, modern software can simulate the theoretical EIS with a given method so that the reverse check could be carried out for the desired circuit.⁵⁵ However, the user should be careful to pick equivalent circuit models to avoid misinterpretation or overfitting since the desired fitting

could be achieved with various proposed models. After selecting the proper circuit model, with the curve fitting the electrodynamics of the system, such as charge transfer behaviour, or double electrical layer, polarization resistance can be understood. The impedance systems can be thought of with distribution in space, so the new elements like Warburg diffusion, Gerischer, constant phase element or Bisquet transmission lines are defined. Those elements are physically and mathematically defined to explain impedance-based difficulties. Double-layer capacitance is a term that defines the distribution of electroactive and charged species that cannot be defined with capacitors since distribution phenomena are not ideal in real-life experiments. For instance, the constant phase element is defined, which takes the phase angle into account. In addition to the constant phase element, the finite Warburg element can be described due to transmission or reflection of the electroactive species depending on the thickness of the diffusion layer.^{55,56}

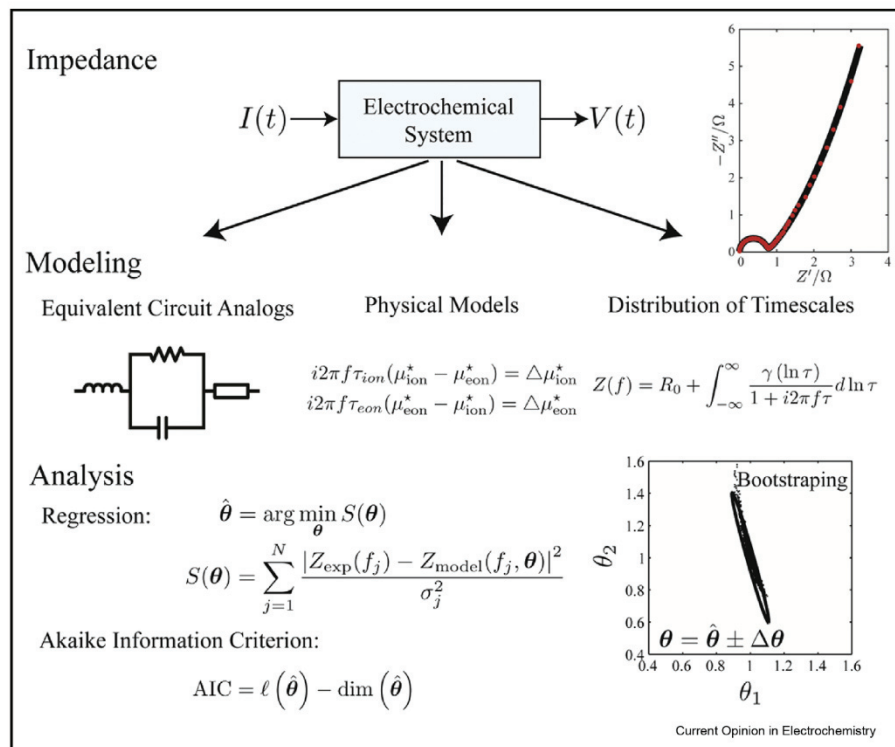


Figure 2.11 General system characterization of electrochemical impedance spectroscopy. (Source: *Current Opinion in Electrochemistry*. Elsevier B.V. February 1, 2019, pp 132–139.)⁵⁴

Figure 2.11 visually describes the analysis of the impedance systems. The data either be explained by equivalent circuit models or differential equation-based models and the distribution of timescales.

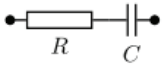
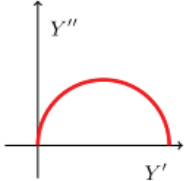
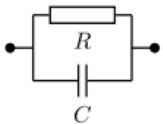
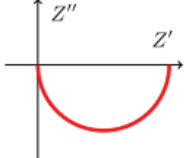
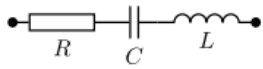
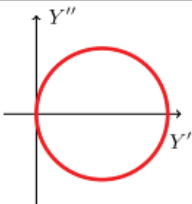
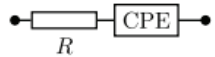
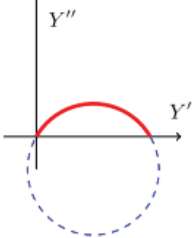
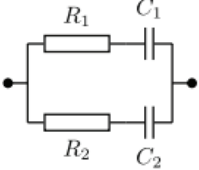
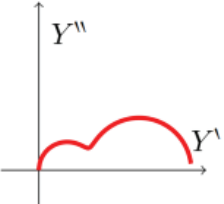
Circuit	Immittance	Nyquist plot	AM solution
<p>Series RC</p> 	$Z = R + \frac{1}{i\omega C}$		$R = \frac{1}{2Y''(\omega_{\max})},$ $C = \frac{2Y''(\omega_{\max})}{\omega_{\max}}.$
<p>Parallel RC</p> 	$Y = i\omega C + \frac{1}{R}$		$R = -2Z''(\omega_{\min}),$ $C = -\frac{1}{Z''(\omega_{\min})\omega_{\min}}.$
<p>Series RLC</p> 	$Z = R + \frac{1}{i\omega C} + i\omega L$		$R = Z(f_{\min}) ,$ $L = \frac{Rf_{\max}}{2\pi(f_{\min}^2 - f_{\max}^2)},$ $C = \frac{1}{L(2\pi f_{\min})^2}.$
<p>Series R-CPE</p> 	$Z = R + \frac{1}{W(i\omega)^\alpha}$		$R = \frac{1}{2Y''(\omega_{\max})},$ $\alpha = \frac{4}{\pi} \times$ $\arctan[2RY''(\omega_{\max})],$ $W = \frac{1}{R\omega_{\max}^\alpha}.$
<p>Two series RC in parallel</p> 	$Z_1 = R_1 + \frac{1}{i\omega C_1},$ $Z_2 = R_2 + \frac{1}{i\omega C_2},$ $Z = Z_1 \parallel Z_2.$		<p>Simple AM solution does not exist</p>

Figure 2.12 Widely used equivalent circuit models for EIS fitting.

(Source: *ACS Biomaterials Science and Engineering*. American Chemical Society 2021.)⁵⁷

Figure 2.12 shows the equivalent circuits in the literature depending on the system, and as seen here, all of the models correspond to a mathematical expression based on the added elements.

2.2.5. Applications of Electrochemical Impedance Spectroscopy

As mentioned in Section 2.2.3, EIS is a robust but easily operated technique that can be used with almost no labelling in various technologies such as surface coatings, fuel-cell, batteries, or even characterization of materials obtained from Mars' surface but most notably in the biosensing area. One of the many advantages of EIS is real-time characterizing or in situ sensing. In this chapter, the applications of electrochemical impedance spectroscopy in the literature will be discussed.

X. Munoz-Berbel et al. carried out the impedimetric characterization of electrode-solution interface via bacterial attachments in 2007. In that work, a three-electrode system was prepared with a platinum disc electrode as a working electrode, Ag|AgCl reference electrode, and a sputtered platinum counter electrode on a SiC surface. They conducted their experiments in 10 Hz to 100 kHz frequency region to detect the changes caused by *E. coli*. First, the growth medium was glucose-containing Minimal Medium AB; then, they plated the bacteria in LB agar plates (10^9 CFU/mL) and diluted it ten times per dilution. The introduction of bacteria to the chips were at 4° C, and experiments were carried out right after the incubation and 40 minutes after the incubation. In order to check the formation, they used epifluorescence microscopy with staining bacteria with 4'-6-diamidino-2-phenylindole (DAPI) in PBS. ⁵⁴

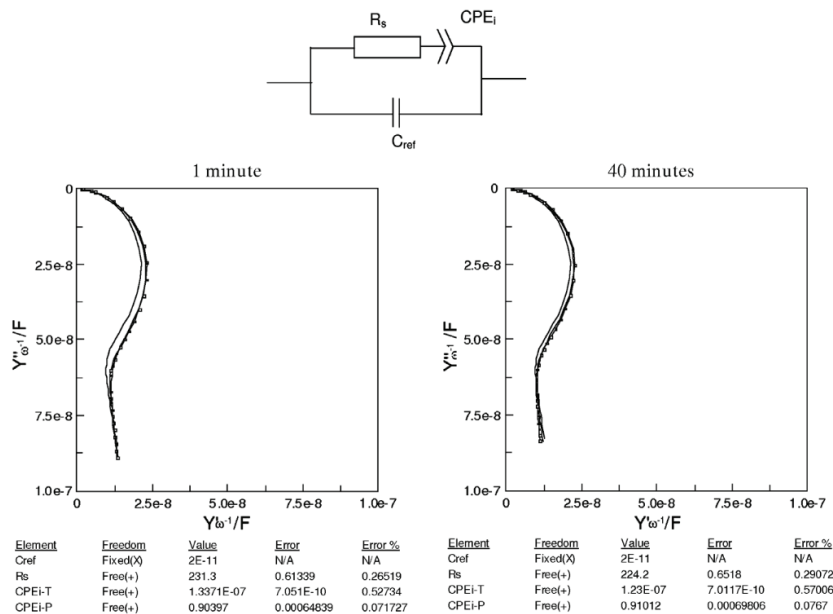


Figure 2.13 Admittance complex measurements carried out by Munoz et al. for *E. coli*

(Source: Electrochem. Commun. **2007**, 9 (11), 2654–2660.)⁵⁴

In Figure 2.13, the EIS spectra and the equivalent circuit is shown. R_s is solution resistance, CPE_i (K_i) is a constant phase element, C_{ref} is for non-faradaic components due to external reference electrode and data were fitted by Z-View software. They found out that K_i was inversely proportional with concentration; with the higher concentrations, this interface CPE value was decreased, as shown in Figure 2.11

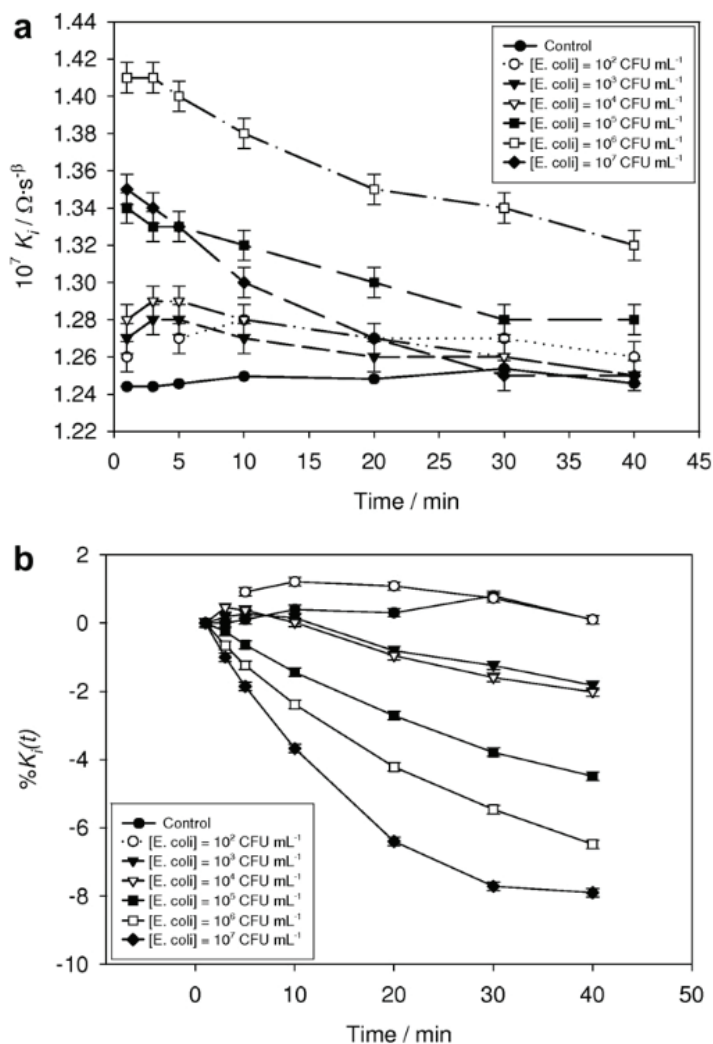


Figure 2.14 Concentration and Time Dependency of K_i

(Source: Electrochem. Commun. 2007, 9 (11), 2654–2660.)⁵⁴

According to Figure 2.14 CPE was changing due to changing the double layer with bacterial attachment. Bacteria are also charged species; the double layer is also persistent around them, so increasing the bacterial concentration will cause a lower Debye length due to increased charge. Another explanation from the article is the surface

coverage. The higher cell concentration will cause a higher attachment to the electrode, as shown in Figure 2.11b.

Moreover, Yoav et al. carried out biofilm experiments with a unique equivalent circuit model with indium tin oxide electrodes within the 100 mHz to 400 kHz range for *E. coli*. Their equivalent circuit model was proposed to understand the impedance of electrodes, the electrolyte and the electrode/biomaterial/electrolyte via fitting. They defined anomalous diffusion of bacteria towards the electrodes for biofilm formation since anything other than bacteria diffuses slower due to interaction between media and the strain. They carried out fluorescence microscopy to also explain the electrode coverage and visualize and demonstrate how bacteria diffuses. The article points out that the initial attachment is responsible for resistance and capacitance changes. The biofilm growth was found to be the reason for intrinsic capacitance and resistance. The bacteria were grown in Luria–Bertani (LB) media, with 0,1 mg/mL ampicillin. While carrying out the impedance experiments provide a polarization with 600 mV, 50 mV, and -500 mV since the double-layer effect on bacteria changes with different voltages. They call out that LB media contains electroactive species that impact the measurements either with chemical interaction or electrostatic forces.⁵⁸

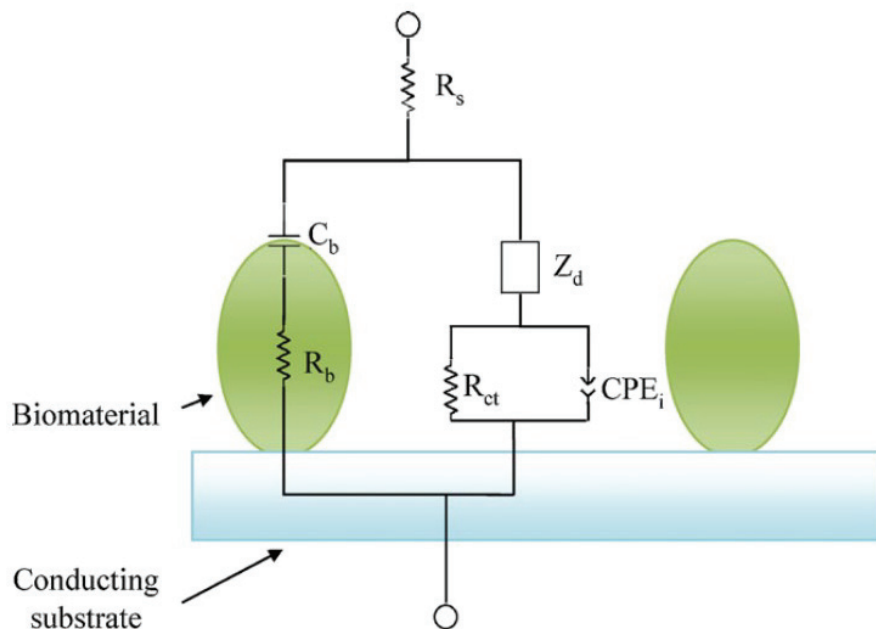


Figure 2.15 The equivalent circuit model to describe biofilm formation by EIS

(Source: *Electrochimica Acta*; 2011; Vol. 56, pp 7780–7786.)⁵⁸

In Figure 2.15, The R_{ct} , R_s and R_b are resistances for charge transfer and biomaterial, C_b is the capacitance for biomaterial, CPE_i is a constant phase element for electrode/solution interaction, Z_d is anomalous diffusion which Bisquert and Compte described in 2001.⁵⁹ They indicated that the capacitive effect resulting from cell growth and attachment increased with time, where the resistive effect decreased. Furthermore, they said that the optical coverage with microscopy results correlates cell attachment towards electrode depending on cell shape and concentration, adequate time constant $\tau_b = R_b \times C_b$ was calculated to prove that the 1D electrical model was not suitable for biofilm formation, so they built the model in Figure 2.12 and fitted the data with using MATLAB software.

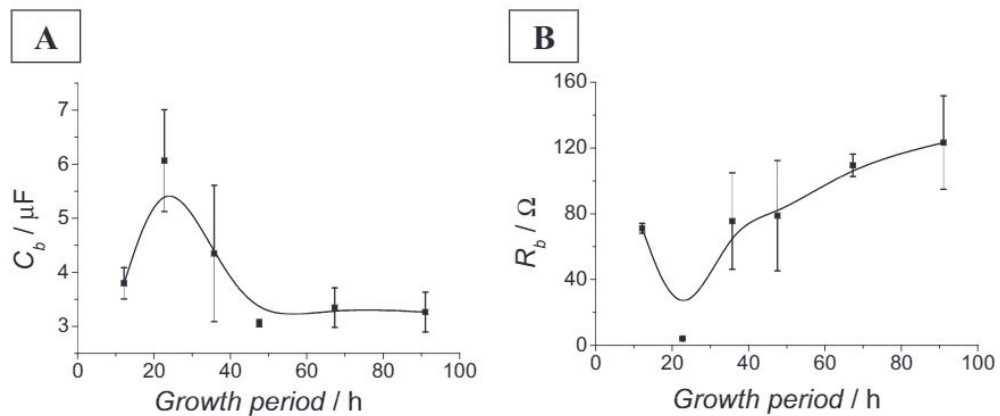


Figure 2.16 Calculated a) capacitive b) resistive dynamics of *E Coli* biofilm

(Source: *Electrochimica Acta*; 2011; Vol. 56, pp 7780–7786.)⁵⁸

Figure 2.16 shows the capacitance and resistance of biomaterial that is calculated via fitting. As shown, bacterial growth and diffusion towards electrodes increase the capacitance about 20h after incubation; then, the capacitance is decreased due to stable coverage of the electrode. The resistive effect was inversely proportional to the capacitance; it decreased in the first 20h, but then it started increasing. The initial bacterial adsorption on the electrode surface and growth covers the electrodes, but with the released extracellular components from bacteria, this capacitive behaviour decreases since the thickness of biofilm increases, unlike the resistive effect, which is behaving reciprocally. They conclude that the different stages of biofilm formation result in different porosity, thickness, and surface coverage on ITO electrodes, and this method is promising not only for prokaryotic cells but also for eukaryotic cells.

In addition to these articles, Liu et al. designed an impedimetric biosensor chip to characterize biofilm formation. Their chip consists of an interdigitated electrode that brings a low ohmic drop, faster steady state, rapid reaction kinetics, and improved signal-to-noise ratio. In that article, they tried to characterize *E. coli* and *Salmonella* species at the same time. They carried out EIS at 1 Hz to 100 kHz with a 100 mV excitation voltage while having 3.5 mm, 2 mm, and 1 mm cavities on PDMS to achieve enough contact area. The results with different cavities show that increasing the cavity area decreases the impedance, so a 3.5 mm chip was used in all their experiments. As they call biofilm formation consists of reversible adhesion stage, irreversible adhesion stage, early-mature stage, mature stage and dispersal stage with impedance spectroscopy those stages were illuminated by the help of equivalent circuit modelling. ⁶⁰

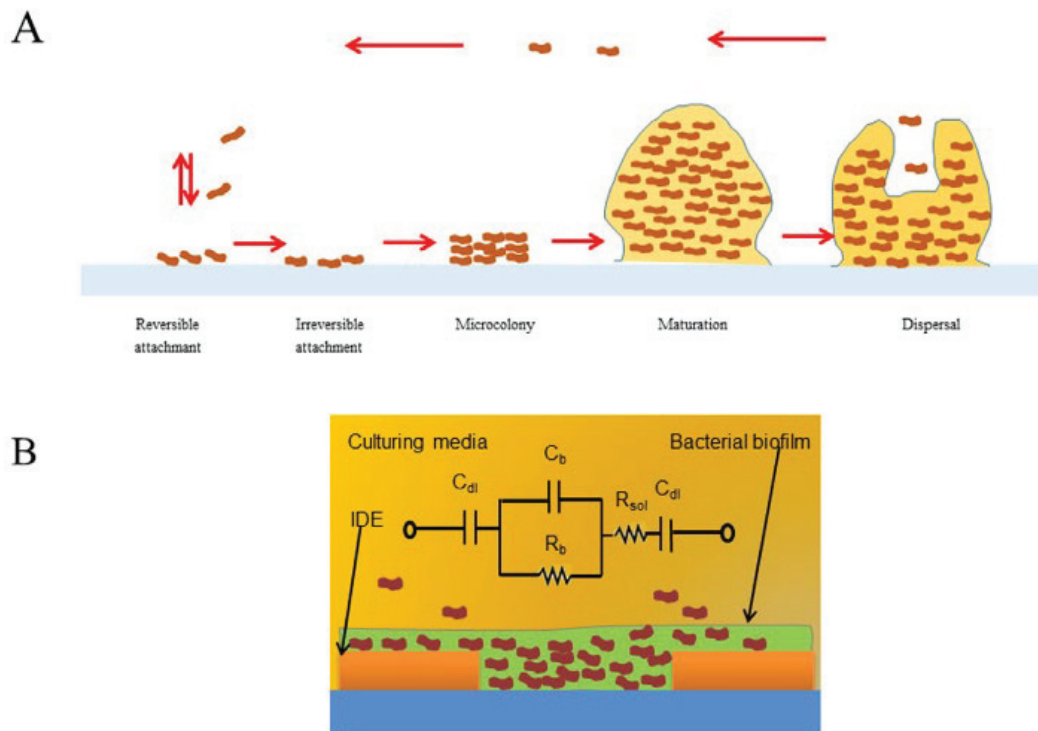


Figure 2.17 Impedance analysis for the biofilms formation process. (A) Stages of biofilms formation process including reversible adhesion stage, irreversible adhesion stage, microcolony stage, mature stage and dispersal stage. (B) The equivalent circuit model for impedance analysis of *Salmonella* and *E. Coli* biofilms.

(Source: Biosens. Bioelectron. **2018**, 112, 86–92.) ⁶⁰

The growth of bacteria and biofilm's maturation stage increase cell adhesion on the electrode while the bacteria produce an extracellular matrix.

The produced ECM increases the resistance, and the biofilm formation decreases the capacitance. They found out that two different impedimetric results were present with *Salmonella* and *E. Coli*. The capacitance of *Salmonella* changes with small fluctuations while the resistance is decreasing. After 30h, the capacitance decreased owing to biofilm formation, extracellular matrix and cellular communications. Their results revealed that *Salmonella* started forming biofilm around 24-48h, and they proposed that after 42h with the consumption of nutrients in the media, bacteria might escape the dense biofilm structure, which results in decreased resistance and increased capacitance.

On the other hand, *E. Coli* shows a sharp decrease in capacitance and increase in resistance due to rapid biofilm formation between 0-12h. Between 12-24h, with the biofilm dispersion, the capacitance is increased while resistance is decreased. With the rebinding of bacteria, capacitance and resistance changed with the same trend.

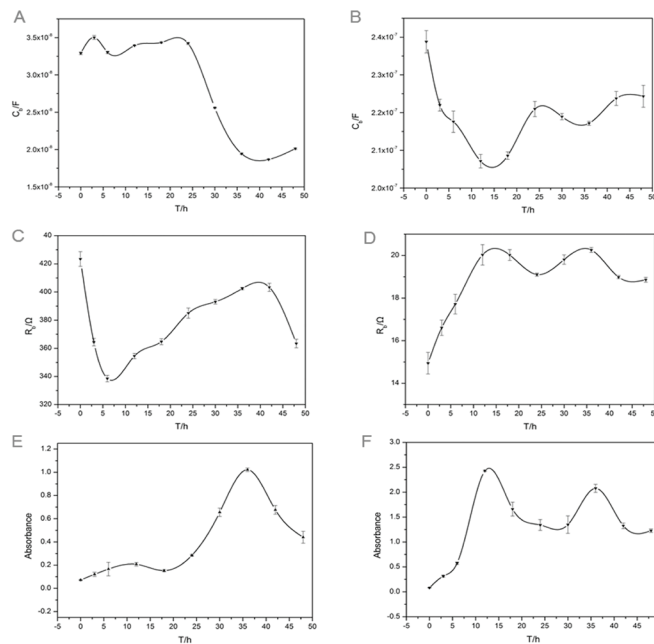


Figure 2.18 Fitting results of the equivalent circuit model for EIS of *Salmonella* and *E. Coli* biofilms as well as the results of Crystal violet staining experiments. (A) Trends of C_b during *Salmonella* biofilms formation process; (B) Trends of C_b during *E. Coli* biofilms formation process; (C) Trends of R_b during *Salmonella* biofilms formation process; (D) Trends of R_b during *E. Coli* biofilms formation process.

(Source: Biosens. Bioelectron. **2018**, 112, 86–92.)⁶⁰

In addition, Song et al. conducted EIS experiments using Au, glassy carbon (CE) and reduced graphene oxide (rGO) modified glassy carbon electrodes. They mentioned that the Au electrode was unsatisfactory due to the small size and less interaction of bacterial cells. Hence, they prepared CE with in situ modification with rGO. The modification simply carried out by drop-casting chemically acquired GO onto CE. With this modified electrode, they analyzed three different bacterial strains, *Streptococcus mutans* (*S. mutans*), *Actinomyces viscosus* (*A. viscosus*), and *Lactobacillus fermentum* (*L. fermentum*) that are oral pathogens. Results stated that using rGO-CE showed higher impedance values than Au and bare CE electrodes, and the Nyquist plot showed only diffusion related impedance since GO is highly conductive with less charge transfer resistance.

Figure 2.18 shows the phase angles and impedance values of biofilm formation with three different electrode setups. They used bare electrode values to extract biofilm impedance by subtracting from the total impedance with that they hypothesize that they calculated the biofilm impedance statistically. As seen in the Figure, bacteria strains showed different impedance and phase values at the same frequencies, but *L. fermentum* had a negative impedance change, so they stated that the Au electrode was not suitable for that strain. Furthermore, they found that the impedance value rose after 12h and 20h, suggesting bacterial attachment and biofilm growth started with those four frequencies of 1.17, 5.47, 11.7, and 54.7 kHz. After calculating those phase changes, they stated that

They modified with rGO-CE showed greater impedance results, and it was more suitable for biofilm analysis than Au or unmodified CE.

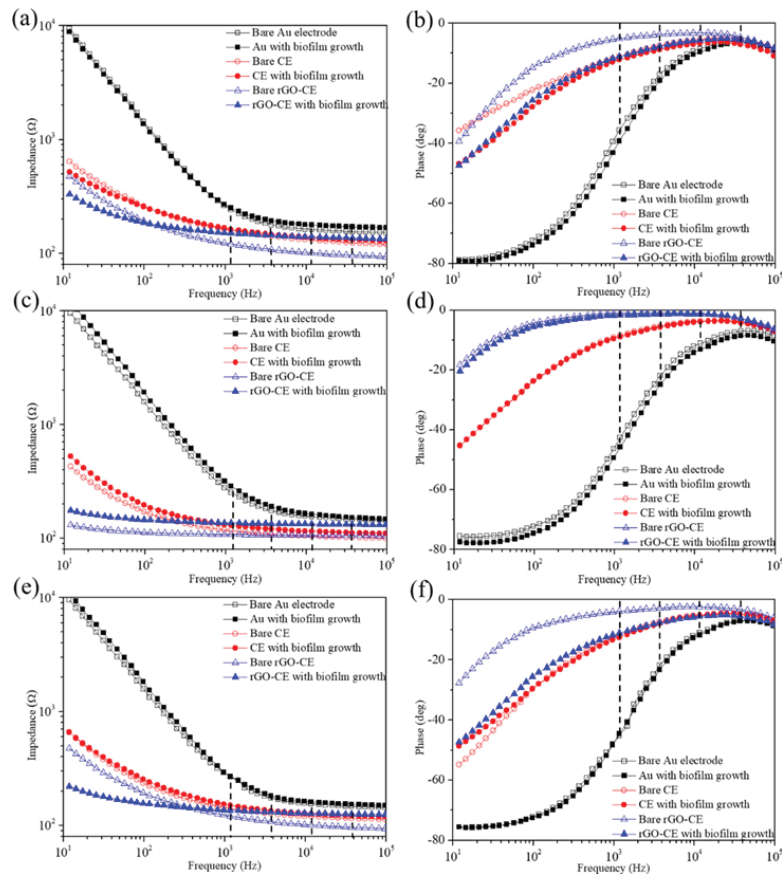


Figure 2.19 Impedance amplitude and phase spectrum of the three kinds of bacteria. Bode impedance spectra of *S. mutans* (a), *A. viscosus* (c), and *L. fermentum* (e) on the Au, CE, and rGO-CE interface. Phase spectra of *S. mutans* (b), *A. viscosus* (d), and *L. fermentum* (f) on the Au, CE, and rGO-CE interface. ⁶¹

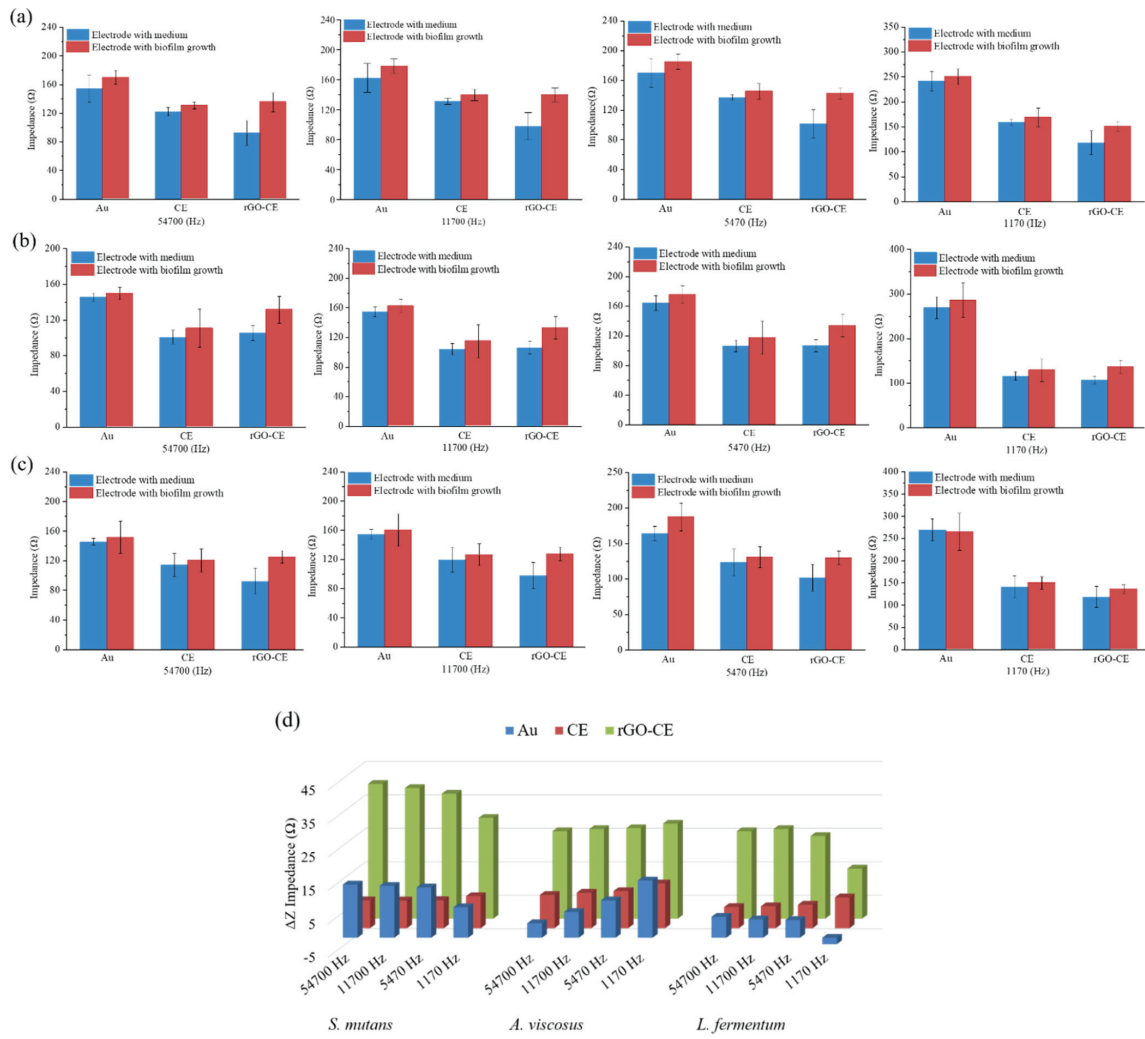


Figure 2.20 Statistical analysis of the impedance values of *S. mutans* (a), *A. viscosus* (b), and *L. fermentum* (c) attached to the surface of the different electrodes before and after biofilm formation. The data represent the mean of five results \pm standard deviation. The ΔZ of the three kinds of bacteria at different frequencies (d)⁶¹

CHAPTER 3

EXPERIMENTAL

3.1. Methods

3.1.1. Bacterial strain and growth conditions

The bacterial strains of *Salmonella Enteritidis* 3934, containing GFP expressing plasmid p2777 and Δ csgD mutants (curli- and cellulose-deficient strain), are referred to as wild type (wt) mutant strains, respectively. Both strains were routinely cultured on Luria-Bertani (LB) agar at 37°C. In preparation for biofilm assays, LB broth without (w/o) salt was used in overnight cultures to inoculate new cultures growing at 37°C under shaking conditions, with optical density recorded at 600 nm.

3.1.2. Electrochemical Measurements

All electrochemical measurements, including square wave voltammetry, open-circuit potential, and impedance spectroscopy, were performed using Gamry Reference 600 potentiostat (Warminster, USA). The three-electrode cell with a boron-doped diamond rod-shaped electrode (Fraunhofer, USA) as a working electrode having 0.02 cm² surface area and platinum wire auxiliary and Ag/AgCl (3 M KCl) reference electrodes (Warminster, USA) was used for all measurements. The 2 mV step size, 10 mV pulse size with 10 Hz frequency were used as a starting parameter for all SWV measurements.

3.1.3. Cleaning of Electrodes

The working electrode was cleaned using a polishing cloth and 3, 1, 0.3, and 0.05 μm alumina powder. First, alumina powder was dusted into the polishing cloth and wetted by deionized water. Then, the electrode was rubbed carefully on the cloth, and the surface was rinsed with water to clean out the residual alumina. Reference and counter electrodes were put into a cleaning detergent and washed with water.

3.1.4. Equivalent Circuit Modelling

Following the EIS analysis to define the biofilm parameters, two different equivalent circuit models were built, and the fitting process was carried out using Gamry Echem Analyst software. For initial input parameters for designated circuit elements, the impedance value of various frequency regions was selected. The high-frequency region (10^4 - 10^5 Hz) where the bode plot had linearity was selected as the solution resistance. Then, Z_{mod} at the low-frequency region (10^{-2} - 10^{-1}) was selected for the polarization resistance. For the constant phase elements, the capacitance was calculated by following Equation 2.⁶²

Here, A corresponds to the capacitance taken from the mid-frequency region (10^{-2} to 10^3 Hz). α is the surface parameter and also includes the phase shift, which means CPE is pure capacitor when $\alpha = 1$ and CPE is a pure resistor when $\alpha = 0$, but in most experiments with solid electrodes, it is between 0 and 1 ($0 < \alpha < 1$).⁶² After calculating the initial parameters, the fitting is conducted using the simplex algorithm on the software. Then with the fitted data, a preinstalled calculation script on the software was used to extract the impedance data for each time interval for both models.

3.1.5. Scanning Electron Microscopy and Sample Preparations

Following impedance analysis, the biofilm samples were collected and placed in a fixation solution (2.5% glutaraldehyde in phosphate buffer saline, PBS pH 7.0). Before critical point drying, to remove glutaraldehyde from the system, samples were washed with deionized water. This process was followed three times, successively. Then, each sample was placed in 30%, 50%, 70%, 95% of ethanol solutions for 10 minutes.

After that, samples were kept in 99.5% ethanol for 15 minutes to achieve slow dehydration, and the latest step was repeated two times. Following the dehydration process, the samples were applied to the automated critical point drying chamber at eight °C and kept under the pressure of 50 bar with continuous stirring in under CO₂ atmosphere. After that, the samples were kept 40 °C under 80 bar pressure without stirring for about 50 minutes. Then the system was gradually degassed, and samples were stored at 37 °C for 30 minutes to dry. Following the drying process, the samples were coated about 150-200 Å with Platinum using a sputtering method to provide better contrast and conductivity for the SEM measurements. All SEM images were acquired using a scanning electron microscope ((Zeiss Ultra 55) using a secondary electron detector with ETH 3.00 kV with a 5-6 mm working distance at different magnifications.

CHAPTER 4

RESULTS AND DISCUSSION

4.1. Experiments in Bulk Solution

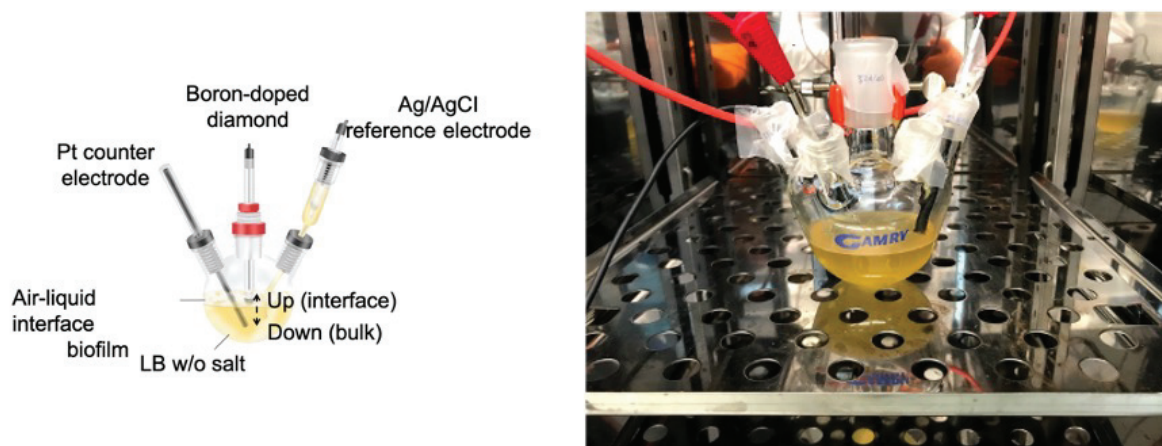


Figure 4.1. General Description of Experimental setup

Figure 4.1 shows the general schematic of the experimental setup. The biofilm wild-type strain, genetically modified strain and LB w/o salt media were filled in a three-neck volumetric flask. To understand the biofilm characteristics, I conducted experiments in the interface and bulk with all three conditions mentioned in Section 1.3.

Electrochemical measurements are carried out with sterilized electrodes and electrochemical cells, and measurements started with 75 mL of LB w/o salt solution in the incubator at 28 °C. 750 μ L (1.0% v/v) of overnight culture was used for both mutant strain and wild-type strain for all electrochemical experiments. First, the BDD electrode has been adjusted to the position where air-liquid biofilm forms and moved the counter and reference electrodes in bulk solution for bulk experiments, and all three electrodes were placed inside the medium.

The LB media without any bacterial contamination were carried out both at the air-liquid interface and bulk as control experiments. Then, to gather biofilm information, a wild type and Δ *csgD* mutant of the same species cannot form biofilm and cannot produce curli, and cellulose Δ *csgD* (cellulose-/curli-) was used to perform the experiments.

The square-wave voltammetry was conducted as a pulsed voltammetric method that is sensitive while extracting capacitive current from the response and lowering detection limits. SWV allows us to conduct faster analysis than other pulsed techniques such as differential pulse voltammetry (DPV) or normal pulse voltammetry (NPV). Moreover, SWV is a method that applies a series of potential pulses with potential changes overlaid with a square wave pulse, with a forward and then reverse pulse occurring on each tread of the ladder, whose basics were shown in Section 2.2.1. Square voltammetry was performed at -1.0 V to +2.5 V. Experiments run for 48h, but the data were collected every 12h starting from 1min.

First, I performed impedance analysis at the open-circuit voltage at a frequency range between 10^{-2} to 10^5 Hz for the wild-type strain. The proposed biofilm model and experimental data with fitting in the Bode plot format (Z_{mod} vs frequency) and (Phase Angle ($^{\circ}$) vs frequency) for the measurement of the strains are proposed in this section. While deciding the equivalent circuit models, the characteristics of a capacitor element at the model depend on the frequency, unlike the resistor by the following equations Z is the impedance, ω is the frequency, R is the resistance, and C is the capacitance. Derived from equations, at the Bode Plot, the low frequency corresponds to the capacitance, and the high frequency corresponds to the resistance.

$$z_C = \frac{1}{j\omega C}$$

$$z_R = R$$

$$z_{CPE} = \frac{1}{Q(j\omega)^n}$$

To fit the experimental data, I defined two different models in two different time intervals as 0-24h and 24-48h, based on our observation and experiments by both eQCM and confocal imaging. Both techniques showed that biofilm started to form and attach to the surface in the time range between 18h-24h. I used the modified Randles circuit as a basic model for the first interval and modified it for biofilm modelling for the second interval of the whole incubation period.

For both models, I defined certain circuit elements such as solution resistance (R_{solution}), polarization resistance ($R_{\text{polarization}}$), charge transfer resistance (R_{CT}), constant phase elements for the electrode ($Q_{\text{electrode}}$), and the double-layer capacitance (Q_{dl}), as well as excessive capacitance ($C_{\text{excessive}}$) in parallel to the whole circuit. The basic model was used to extract the principal solution parameters such as charge transfer resistance and double-layer capacitance parameters after fitting EIS data. According to the fitting parameters, both charge-transfer resistance and double-layer capacitance increased gradually at the early stage of bacterial growth (0-12h). These parameters were used to define electrochemical properties at the electrode-solution interface; however, I also used the biofilm model to define biofilm contribution. In this model, two additional circuit components, capacitance (C_{biofilm}) and resistance (R_{biofilm}), were introduced for the 36h and 48h of measurements since biofilm also causes extra resistivity and stores electrical charges on the electrode interface once it forms. To test the validity of the proposed biofilm model, I first applied the basic model (without C_{biofilm} and R_{biofilm} components) on 24h, 36h, 48h data, and the results showed very low goodness of fit with a high percentage of error. Therefore, I used the biofilm model, which involves biofilm-electrode and biofilm-solution interface, to define biofilm contribution to charge-transfer resistance (R_{biofilm}) and double-layer capacitance (C_{biofilm}) parameters for 24h, 36h, and 48h.

4.1.1. Square Wave Voltammetry

SWV was carried out in bulk solution for all three conditions starting with wild type strain throughout understanding biofilm formation's electrodynamics. Figure 4.2 shows the square wave voltammogram of wild type strain and a 2 mV step size and 10 mV pulse size with 10 Hz frequency. The voltage was swept between -1.0 V to +2.5 V, and the results show that formed biofilm at the air-liquid interface does not affect the bulk solution, as peaks denoted as Redox I and Redox II are present in the mutant strain and LB w/o salt. Figure 4.2 shows the square wave voltammograms in three conditions.

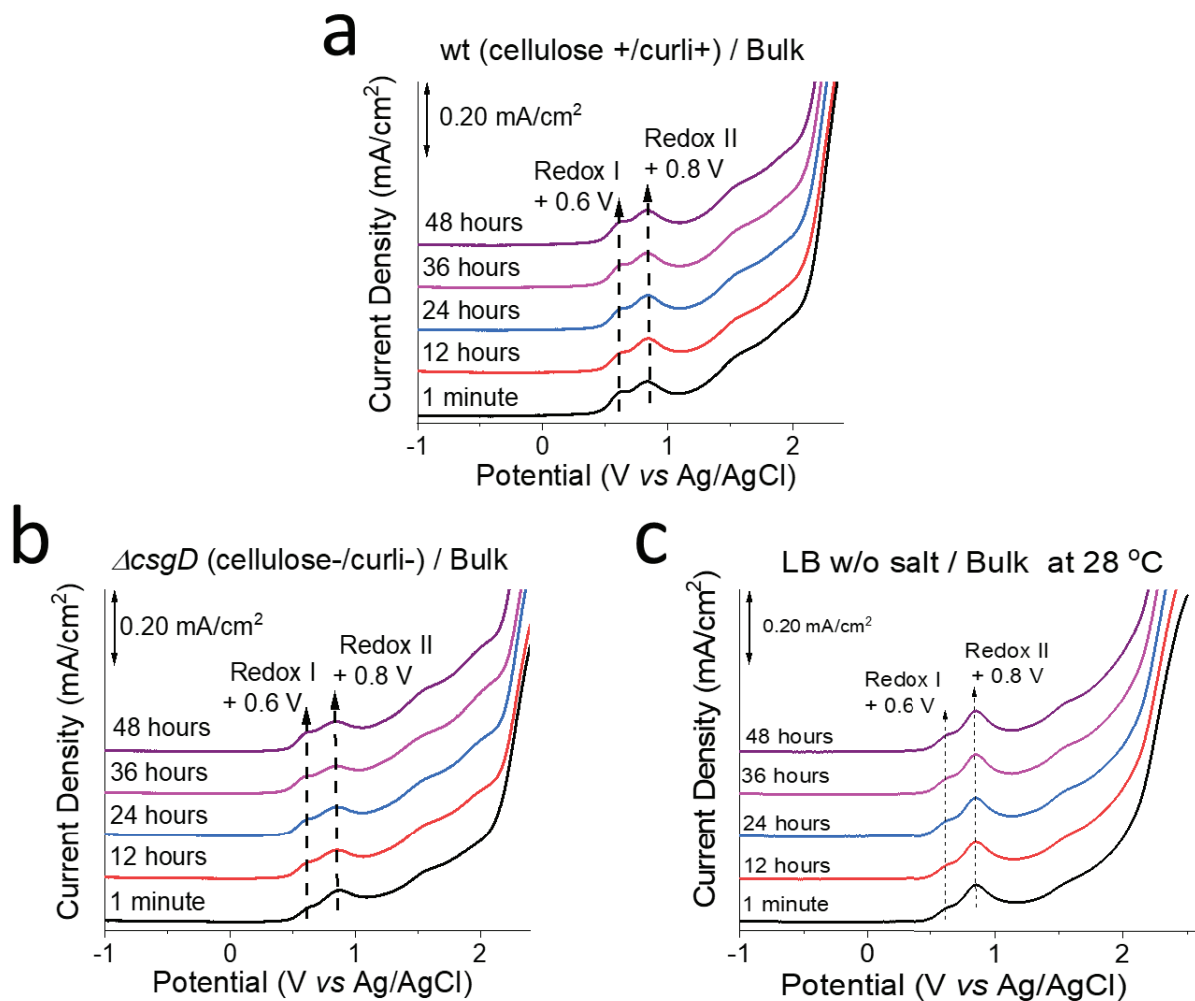


Figure 4.2 Square Wave Voltammogram of the bulk experiments of three conditions. a) wild type strain b) mutant strain c) LB w/o salt

The formation of the biofilm occurs in the air-liquid interface. Two redox peaks are observed at +0.6 V and 0.8 V, but the biofilm formation does not change the solution. With the biofilm formation, bacteria did not produce redox compounds that are released toward the growth medium. The occurred peaks might result from the ingredients of LB w/o salt since bacterial growth did not change the redox peaks. For further investigations, OCP experiments were conducted to analyze potential changes while the bacterial growth in the same experimental setup. OCP results will be explained in the next Chapter 4.1.2.

4.1.2. Open Circuit Potential

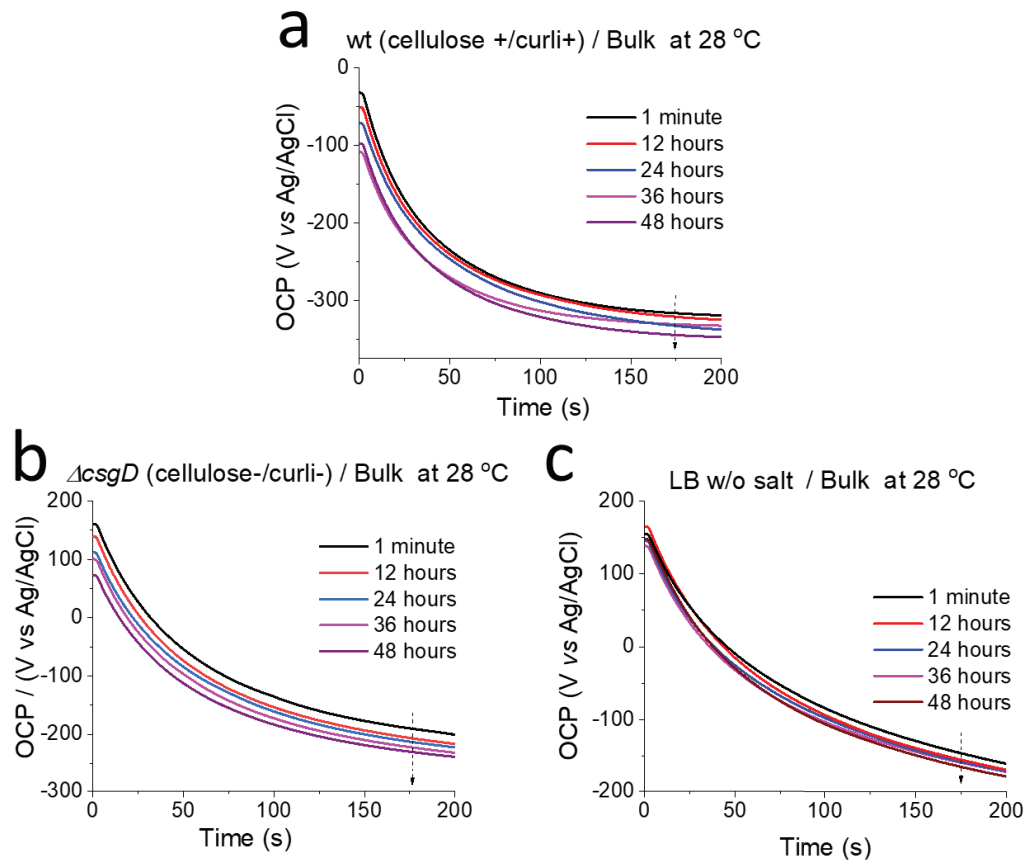


Figure 4.3 Open Circuit Potentials of the bulk experiments of three conditions. a) wild type strain b) mutant strain c) LB w/o salt

As Figure 4.3 and Figure 4.4 proposes, While the change in OCP of LB w/o salt is ± 10 mV, the wild type and the mutant strain had a change of ± 20 mV, these data points were taken from the software, and Figure 4.3 shows the trend of changes in OCP with three conditions. The bacterial growth shifts the OCP in ± 10 mV range, and biofilm formation does not significantly affect the resting potential between reference and working electrode, as demonstrated in Figure 4.4

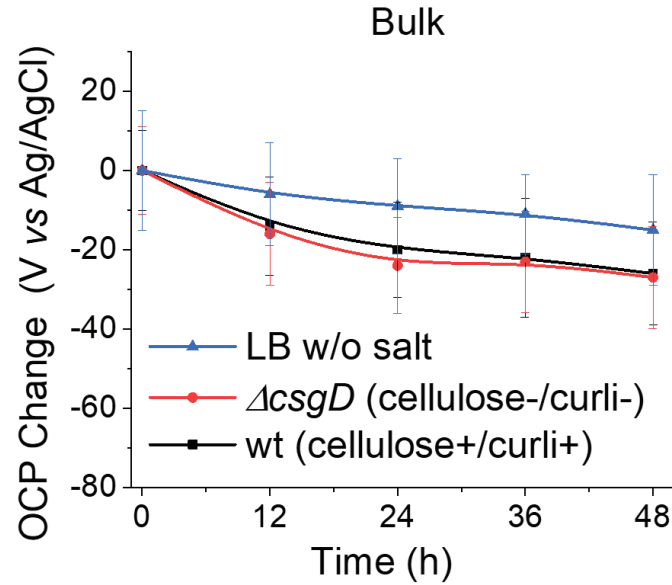


Figure 4.4 OCP Changes of three conditions

4.1.3. Electrochemical Impedance Spectroscopy

To fit the experimental data, I defined two different models in two different time intervals as 0-24h and 24-48h, based on our observation and experiments by both eQCM and confocal imaging. Both techniques showed that biofilm started to form and attach to the surface in the time range between 18h-24h. I used the Randles circuit as a basic model for the first interval and modified it for biofilm modelling for the second interval of the whole incubation period. For both models, I defined certain circuit elements such as solution resistance (R_{solution}), polarization resistance ($R_{\text{polarization}}$), charge transfer resistance (R_{CT}), constant phase elements for the electrode ($Q_{\text{electrode}}$), and the double-layer capacitance (Q_{dl}), as well as excessive capacitance ($C_{\text{excessive}}$) in parallel to the whole circuit. The basic model was used to extract the principal solution parameters such as charge transfer resistance and double-layer capacitance parameters after fitting EIS data, as shown in the goodness of fit with high percentage error, which indicated that data produced for mutant strain and growth media were not relevant for biofilm modelling.

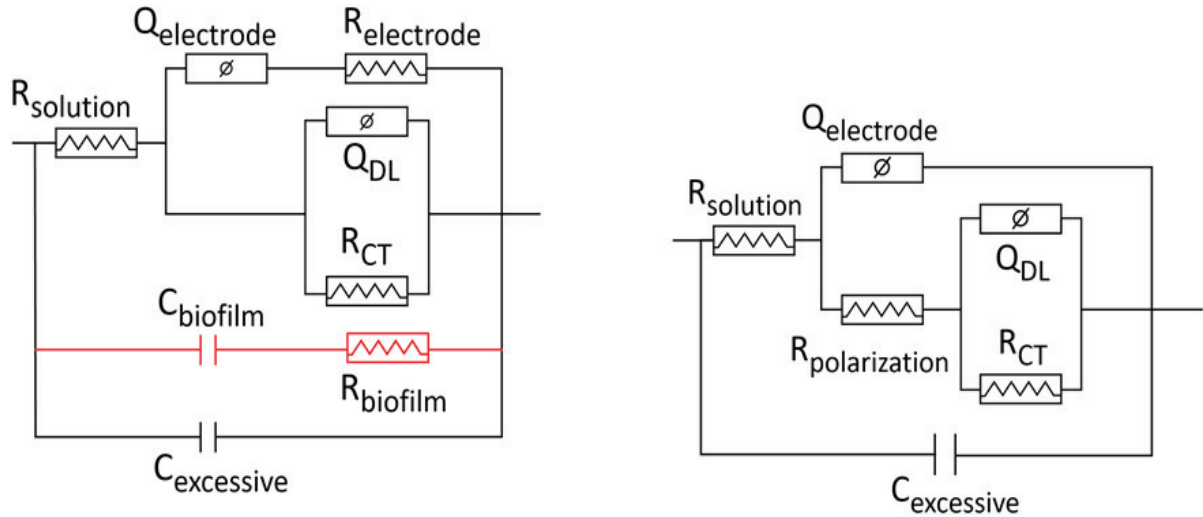


Figure 4.5 Equivalent Circuit Models for Impedance data fitting biofilm model is on the left, and bulk model is on the right

Besides, I also performed impedance analysis for the mutant strain and LB w/o salt using the same experimental conditions for wild-type strains. I proposed Model I for the mutant strain and impedance analysis in different frequencies in the Bode plot format and fitting parameters using the interface setup.

As Figure 4.6 presents, the impedance measurements were carried out for wild type strain in the bulk solution, and the biofilm was formed at the air-liquid interface. The hypothesis that was questioned here was, “what is the effect of biofilm formation on the solution?” I carried out the experiments from 10^{-2} Hz to 10^5 Hz. Data were collected every 12h; since the biofilm was formed at the interface, the equivalent circuit model does not contain biofilm components as no changes were observed with SWV and OCP. The data in Figure 4.4a were fitted according to the model shown in Figure 4.4b. The extracted results have been displayed in Figure 4.4c and 4.4d; two principal parameters were focused on here, double-layer capacitance and charge transfer resistance that is reasoned from solution-electrode, biofilm/bacteria-electrode, biofilm/bacteria-solution interfaces. The charge-transfer resistance and double-layer capacitance values extracted from impedance modelling based on the interactions of interfaces. The double-layer capacitance did not show any deviation since the software’s algorithm shows zero deviation using a constant phase element.

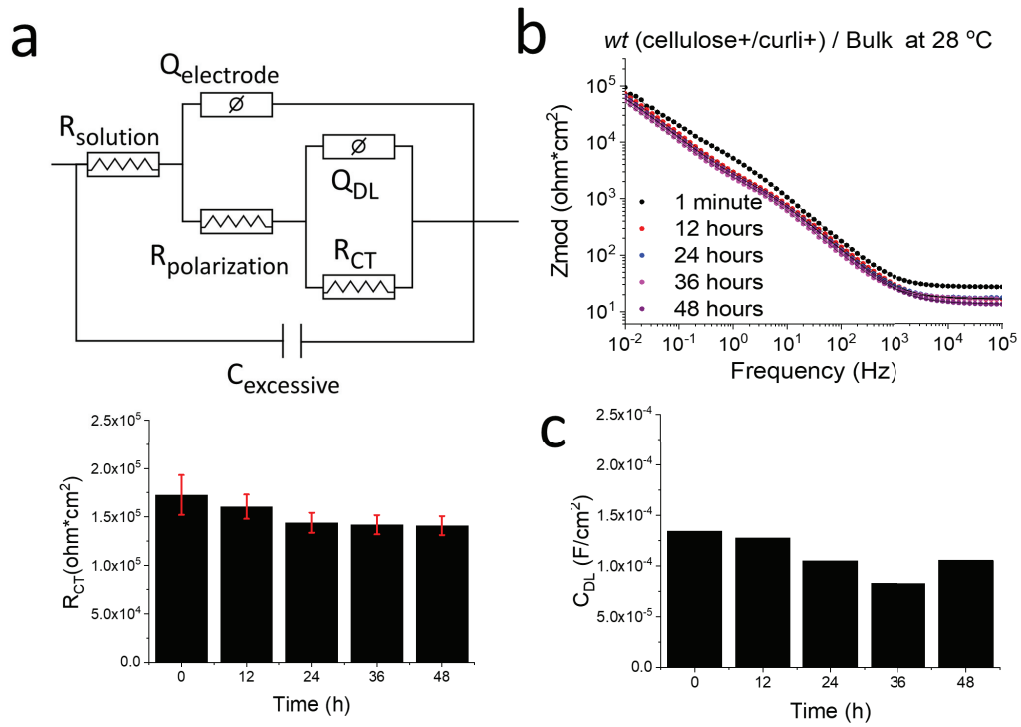


Figure 4.6 EIS experiments for wild type strain in bulk a) equivalent circuit model for EIS fitting b) Bode plot of EIS c) extracted charge transfer resistance d) extracted double-layer capacitance

In this case, the first 12h bacteria start to grow, and both R_{ct} and C_{dl} show a decline from $1.73 \pm 0.205 \text{ M}\Omega \cdot \text{cm}^2$ to $1.60 \pm 0.126 \text{ M}\Omega \cdot \text{cm}^2$ and from $0.134 \mu\text{F}/\text{cm}^2$ to $0.127 \mu\text{F}/\text{cm}^2$, respectively. Since the biofilm sticks together by fibrous cellulose and curli, the aggregates started after 22-24h; the R_{ct} and C_{dl} decreased to $1.44 \pm 0.104 \text{ M}\Omega \cdot \text{cm}^2$ and $0.105 \mu\text{F}/\text{cm}^2$ due to electrode coverage. After that point, R_{ct} shows a stable trend with a slight reduction to $1.41 \pm 0.0977 \text{ M}\Omega \cdot \text{cm}^2$ at 48h due to the slowed growth and biofilm formation. However, C_{dl} keeps decreasing until 36h to $0.121 \mu\text{F}/\text{cm}^2$, then increases to $0.1056 \mu\text{F}/\text{cm}^2$. This phenomenon might result from the consumption of ECM components as nutrition so that bacteria can diffuse into solution by leaving the biofilm due to reduced force caused by fibrous cellulose and curli.

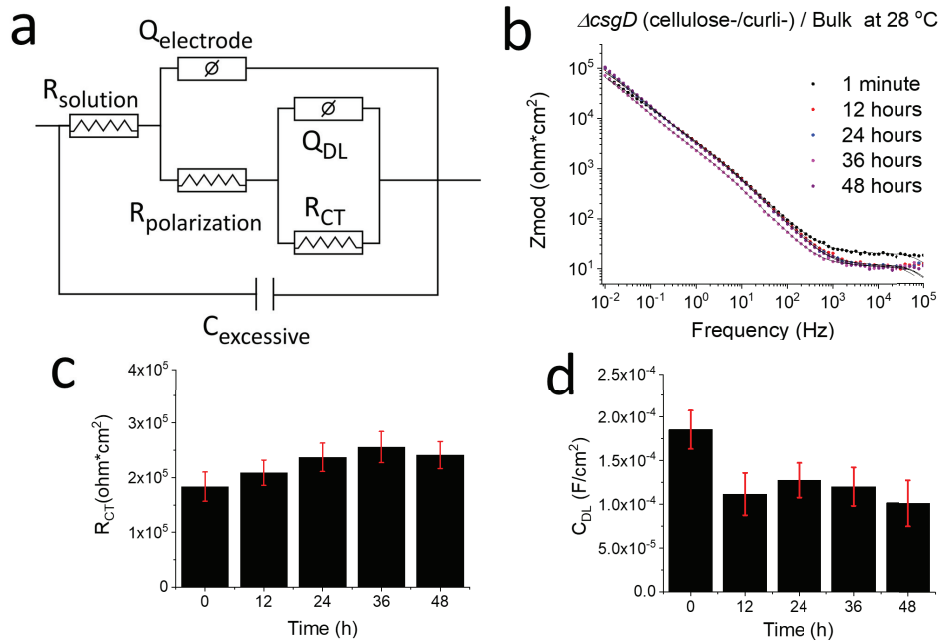


Figure 4.7 EIS experiments for mutant strain in bulk a) equivalent circuit model for EIS fitting b) Bode plot of EIS c) extracted charge transfer resistance d) extracted double-layer capacitance

On the other hand, the trend of R_{ct} and C_{dl} was different for the mutant strain. Bacterial maturation is the main reason for the shifts observed in the solution since the mutant cannot form a biofilm. For the first 24h, the maturation increases the R_{ct} from $1.84 \pm 0.27 \text{ M}\Omega \cdot \text{cm}^2$ to $2.37 \pm 0.26 \text{ M}\Omega \cdot \text{cm}^2$, and it continues rising until 36h owing to bacterial assemble as clusters. For the 48h, R_{ct} decreases to $2.41 \pm 0.25 \text{ M}\Omega \cdot \text{cm}^2$. This change might be attributable to the small dispersion of bacteria inside the solution. As R_{ct} increases, C_{dl} starts to decline from $0.185 \mu\text{F}/\text{cm}^2$ to $0.111 \mu\text{F}/\text{cm}^2$. As aggregation and the growth progress, lack of ECM components in the mutant strain, C_{dl} had small fluctuations, but compared to the wild-type results were minor, as shown in Figure 4.6.

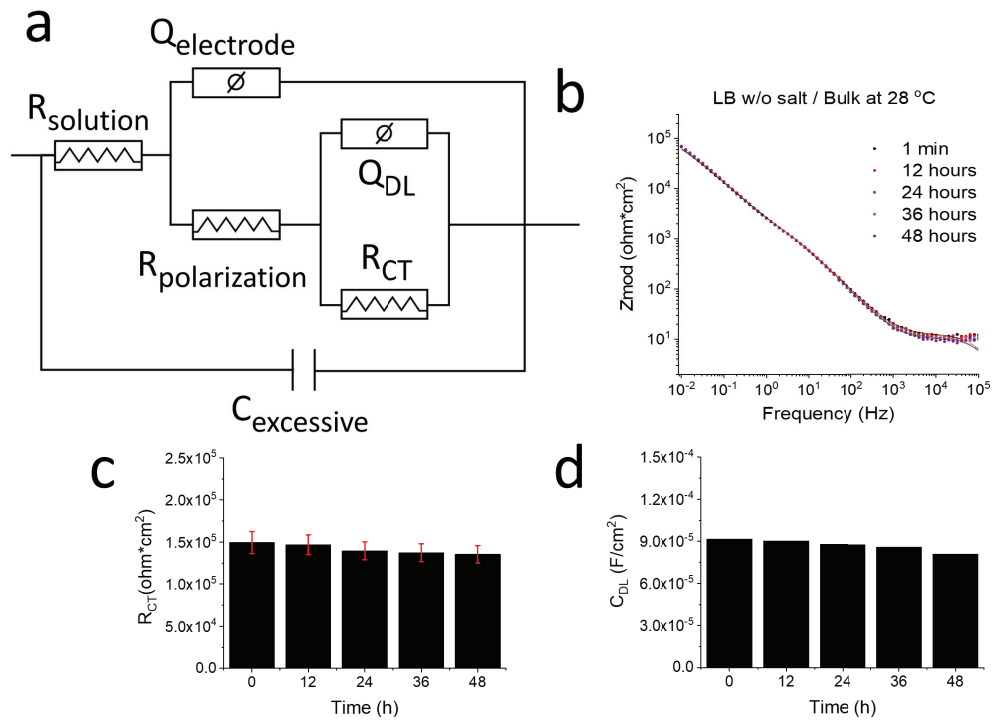


Figure 4.8 EIS experiments for LB w/o salt in bulk a) equivalent circuit model for EIS fitting b) Bode plot of EIS c) extracted charge transfer resistance d) extracted double-layer capacitance

The LB w/o salt experiments fitting showed a stable trend with almost negligible changes than mutant and wild type for both R_{ct} and C_{dl} illustrated in Figure 4.6b,c. For the bulk experiments, both R_{ct} and C_{dl} decreased from $1.45 \pm 0.130 \text{ M}\Omega \cdot \text{cm}^2$ to $1.36 \pm 0.104 \text{ M}\Omega \cdot \text{cm}^2$ and from 0.0916 to 0.0811 $\mu\text{F}/\text{cm}^2$, respectively. Those changes were almost negligible compared to wild-type or mutant strains since no bacteria exists inside the solution.

4.2. Experiments at the Air-Liquid Interface

The EIS experiments were conducted at the air-liquid interface with the same experimental procedure to understand the formation. This part of the thesis will demonstrate the results gathered from biofilm formation for wild type strain, mutant strain and LB w/o salt medium.

4.2.1. Square Wave Voltammetry

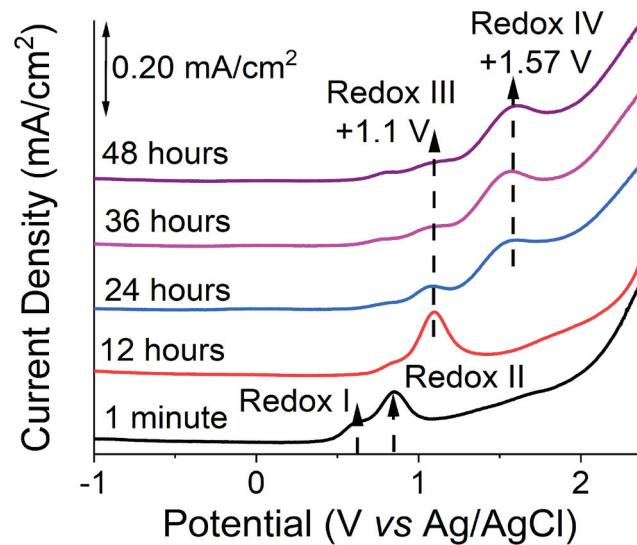


Figure 4.9 Square Wave Voltammetry of wild type strain at the air-liquid interface

The results show that the solution contains wild-type strain possesses two redox peaks positioned at +0.6 V and +0.8 V at the beginning of the incubation, as shown in Figure 4.7. However, after 12h incubation, the current density of these peaks started to decrease while the new strong redox peak appears at +1.1 V (Redox III). The new redox activity appeared at 24h of incubation at +1.57 V (Redox IV), while the peak current density at +1.1 V lessened significantly after 12h. The elevation at +1.57 V stayed stable for 24h, 36h, and 48h of incubation. On the other hand, when the same experiment run for mutant strain in interface setup, the redox peaks at +0.6 V and +0.8 V do not change throughout 48h incubation, and no new redox activity observed. The same redox peaks (Redox I & II) and peak current densities were also observed for the bulk measurements of the wild-type Figure 4.3 and in both bulk and the interface setups of mutant strains and only LB w/o salt medium Figure 4.10.

Peaks for the interface measurement of the wild-type strain occur at the high potential region +1.1 V and +1.57 V, where no bacterial metabolites or any surface proteins are expected to be actively reduced or oxidized. This observation might be possibly caused by the presence of different redox-active molecules secreted by a bacterium potentially used for inter or intracellular communications or regulating the biofilm formation process. However, identifying or isolating those molecules that cause redox activities is hard to achieve at this stage.

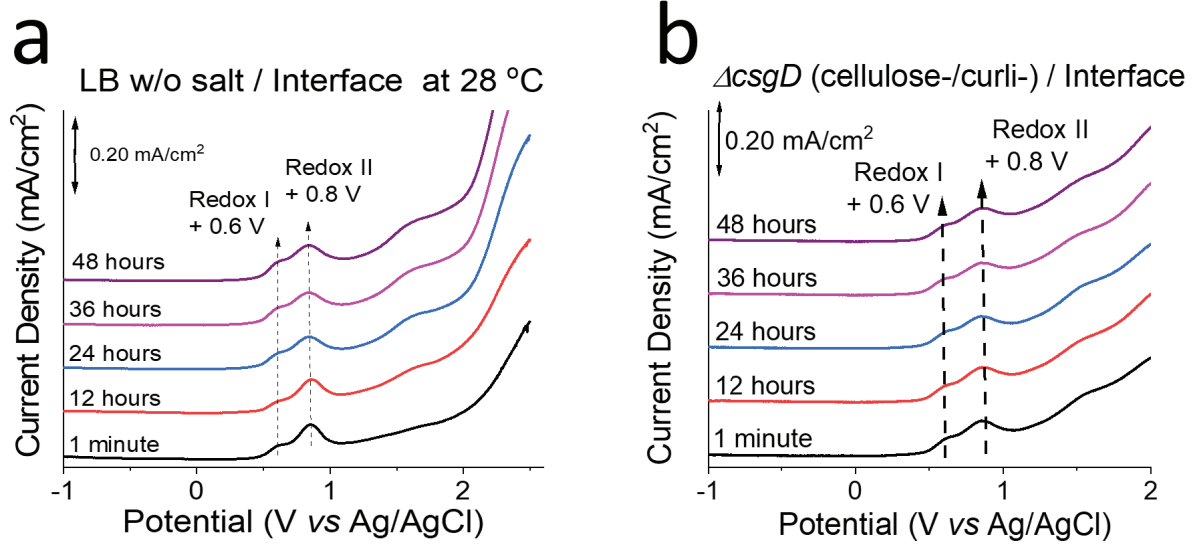


Figure 4.10 Square wave voltammetry for a) LB w/o salt b) mutant strain

As shown here in Figure 4.8 and Figure 4.9, mutant strain and LB w/o salt show identical results with the bulk region; Redox I and Redox II peaks are persistent throughout the experiment. The lack of Redox III and Redox IV shows that biofilm formation has unique redox properties, but the isolation process cannot be carried out with the current methodologies.

4.2.2. Open Circuit Potential

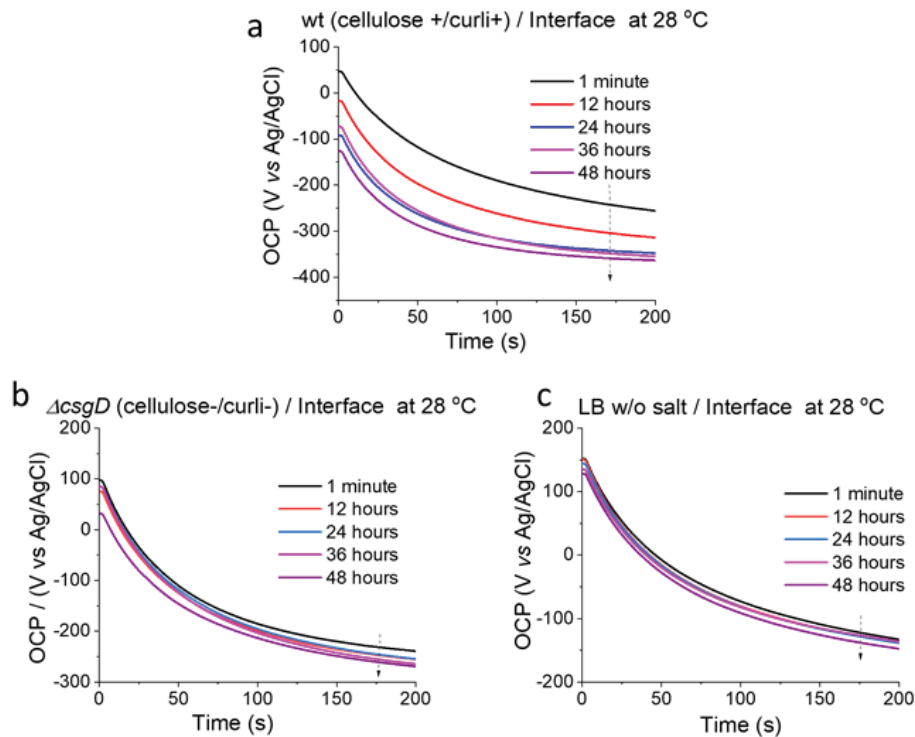


Figure 4.11 Open Circuit Potential measurements for three conditions in the air-liquid interface. a) wild type b) mutant strain c) LB w/o salt

The results for the interface measurements show that wild-type strain has a more significant change in OCP (-118.3 ± 13.2 mV) compared to changes for mutant strains (-29.7 ± 15.2 mV) and LB w/o salt medium (-14.5 ± 9.4 mV), as demonstrated in Figure 4.11 and 4.12, respectively. These results indicate that biofilm formation changes the resting potential between WE and RE, as bacteria first matures, then aggregates, and the bacteria stick together with the extracellular matrix components, unlike the mutant strain and LB w/o salt since observed the mutant strain behaves almost identical in the air-liquid interface and the solution.

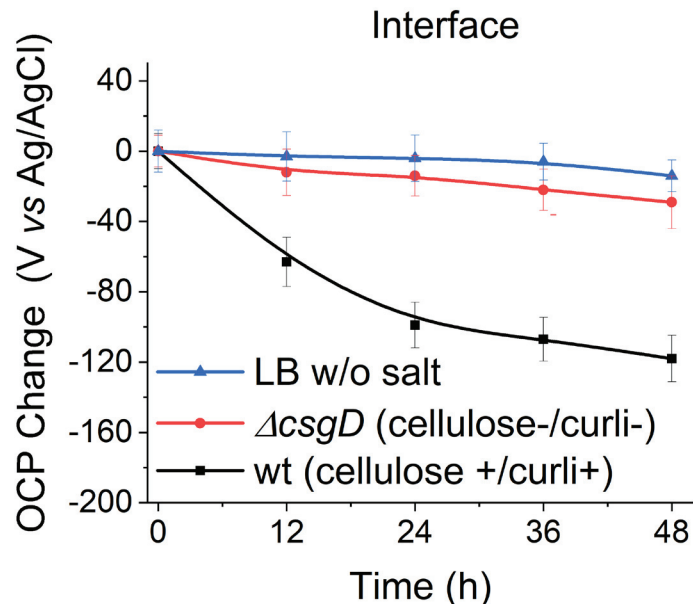


Figure 4.12 OCP Changes of three conditions

4.2.3. Electrochemical Impedance Spectroscopy

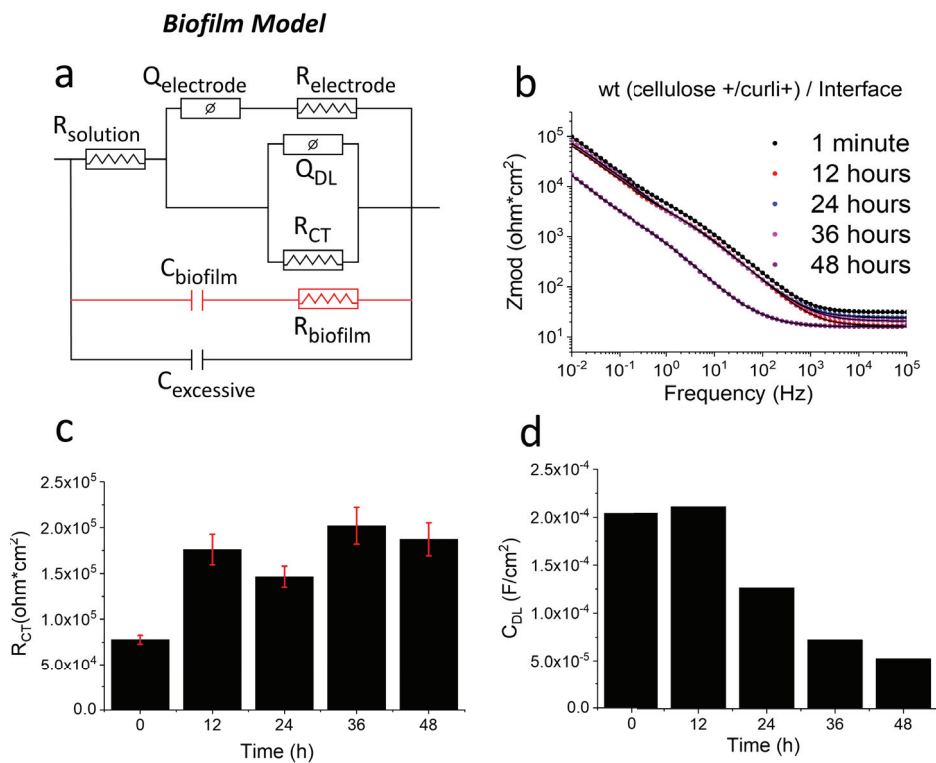


Figure 4.13 EIS experiments for wild type strain in the air-liquid interface a) equivalent circuit model for EIS fitting after 24h b) Bode plot of EIS c) extracted charge transfer resistance d) extracted double-layer capacitance

Figure 4.13b shows the Bode Plot of EIS data of biofilm formation at the air-liquid interface for the wild type bacterial solution. Acquired data is used for fitting, the equivalent circuit model for the first 24h is shown. For the first 24h, the bulk model was used to extract data after fitting of EIS, but after biofilm started forming, the fitting model was changed to gather resistivity and capacitance changes of biofilm formation; Figure 4.13a was built. The added elements to the equivalent circuit model are pointed out. Although the capacitance was calculated instead of using a pure capacitor, the constant phase element was added to the model to factor in the surface roughness and small electrode resistance since it calculates the phase shift caused by those parameters. Figure 4.13c-d shows the effect of bacterial maturation and the development of biofilm on the air-liquid interface. The growth of bacteria causes an increase at both R_{ct} from $0.776 \pm 0.0478 \text{ M}\Omega \cdot \text{cm}^2$ to $1.761 \pm 0.166 \text{ M}\Omega \cdot \text{cm}^2$ and C_{dl} $0.204 \mu\text{F}/\text{cm}^2$ to $0.211 \mu\text{F}/\text{cm}^2$ in the first 12h. Due to biofilm formation, C_{dl} showed a slight decrease until 48h from $0.126 \mu\text{F}/\text{cm}^2$ to $0.0523 \mu\text{F}/\text{cm}^2$. R_{ct} increased from $1.465 \pm 0.1154 \text{ M}\Omega \cdot \text{cm}^2$ to $1.874 \pm 0.1807 \text{ M}\Omega \cdot \text{cm}^2$ due to produced extracellular matrix components. Figure 4.13 indicates the changes in resistance and capacitance of added elements in the modified model for biofilm formation. The resistance and capacitance of ECM components decreased in the 36-48h interval from $9.27 \pm 0.945 \text{ M}\Omega \cdot \text{cm}^2$ to $0.152 \pm 0.0622 \text{ M}\Omega \cdot \text{cm}^2$ and $19.55 \mu\text{F}/\text{cm}^2$ to $1.62 \mu\text{F}/\text{cm}^2$, respectively.

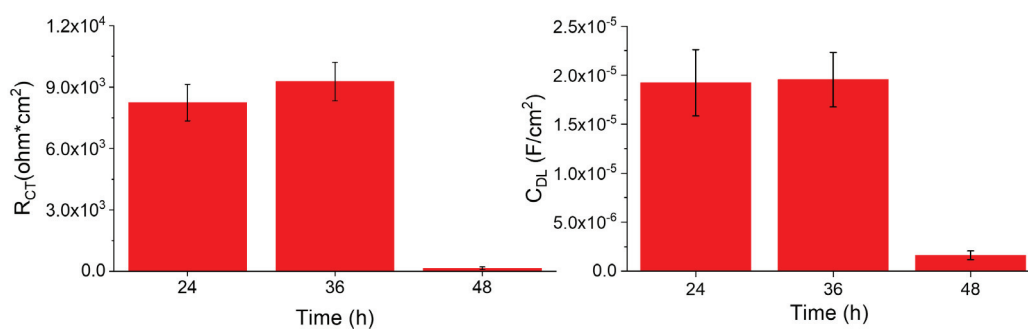


Figure 4.14 Extracted C_{poly} and R_{poly} values according to added circuit elements

To show the electrochemical understanding of biofilm development at the air-liquid interface, as mentioned before, a mutant strain that cannot form biofilm is used in EIS. The Bode plot of the analysis is given in Figure 4.15b. The fitting process was carried out with the model in Figure 4.15a. In Figure 4.15c-d, R_{ct} and C_{dl} parameters are shown. Compared to wild-type changes in R_{ct} and C_{dl} for the mutant strain, shifts were less

dramatic here since the extracellular matrix components of biofilm were not produced in the interface. R_{ct} is increased from $2.607 \pm 0.4512 \text{ M}\Omega \cdot \text{cm}^2$ to $2.93 \pm 0.476 \text{ M}\Omega \cdot \text{cm}^2$ in the first 12h because of the bacterial maturation. After the growth, a decrease is observed until 24h to $2.654 \pm 0.391 \text{ cm}^2$ because of cellular dispersion. Then, it increases slightly to $2.93 \pm 0.472 \text{ M}\Omega \cdot \text{cm}^2$ for the 48h when the cell aggregates form. The C_{dl} is increased 1min to 12h from $0.136 \mu\text{F}/\text{cm}^2$ to $0.152 \mu\text{F}/\text{cm}^2$. After 12h, the C_{dl} followed a decrease until 36h to $0.131 \mu\text{F}/\text{cm}^2$ since the effective area of the WE is decreased with the dispersion of growth bacteria towards the solution. Finally, due to cellular aggregates and clusters of the mutant raised C_{dl} to $0.172 \mu\text{F}/\text{cm}^2$.

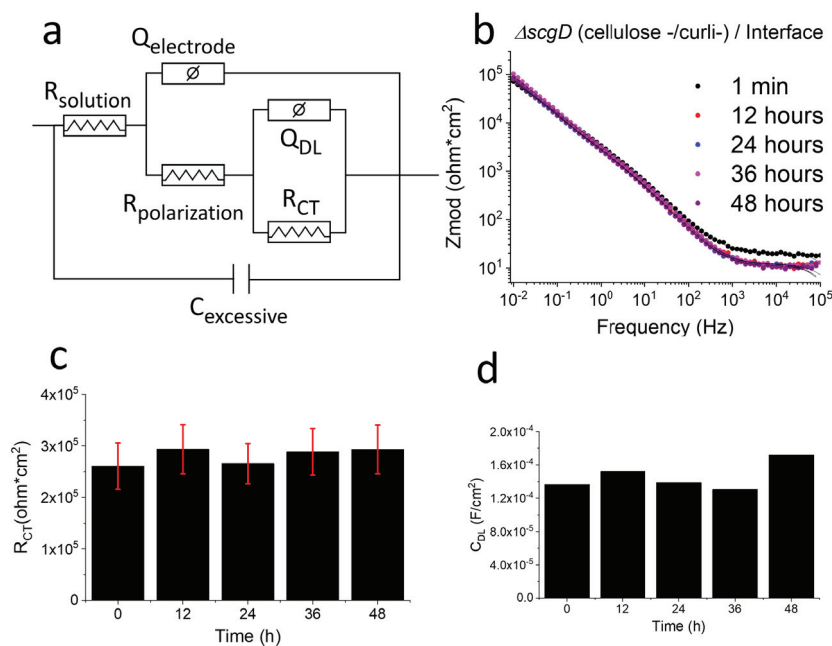


Figure 4.15 EIS experiments for mutant strain in the air-liquid interface a) equivalent circuit model for EIS fitting b) Bode plot of EIS c) extracted charge transfer resistance d) extracted double-layer capacitance

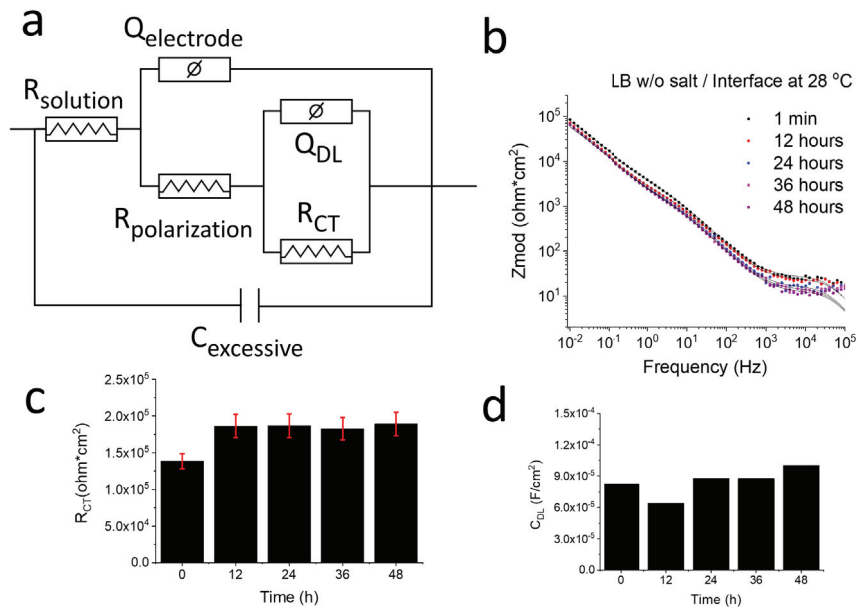


Figure 4.16 EIS experiments for LB w/o salt in the air-liquid interface a) equivalent circuit model for EIS fitting b) Bode plot of EIS c) extracted charge transfer resistance d) extracted double-layer capacitance

Additionally, LB w/o salt medium to understand interfacial electrochemical parameters was performed to measure the bulk circuit model. The results show that all solution parameters, including charge-transfer resistance double-layer capacitance, do not change more than 10% of their initial value during 48h of incubation for both interface and bulk measurements, as shown in Figure 4.16

4.3. Scanning Electron Microscopy

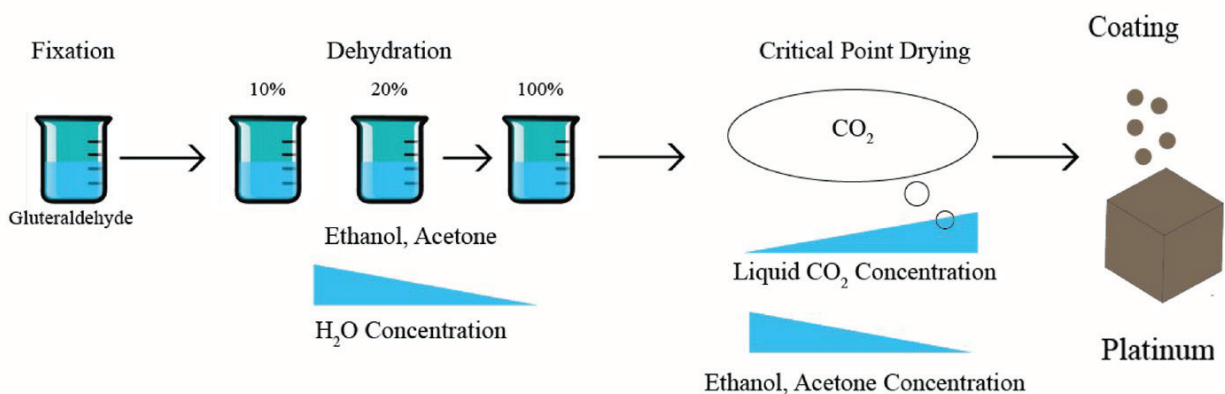


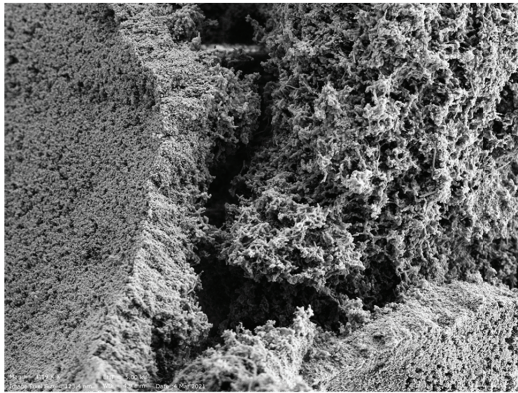
Figure 4.17 Schematics of Critical Point Drying Process (CPD)



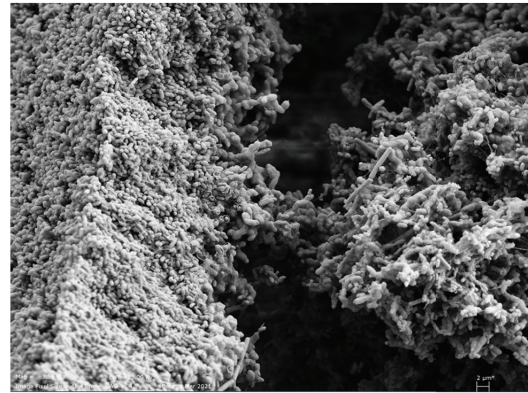
Figure 4.18 On the left Isolated biofilm after the experiment and on the right, re-dispersion in deionized water

Figure 4.18 shows biofilm taken from the air-liquid interface at the end of the experiment for scanning electron microscopy. Also, to observe the water effect, the biofilm was dispersed in deionized water.

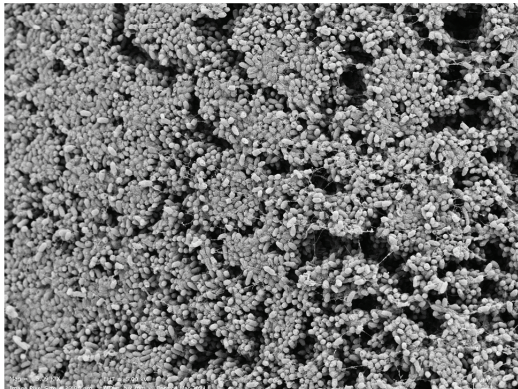
a



b



c



d

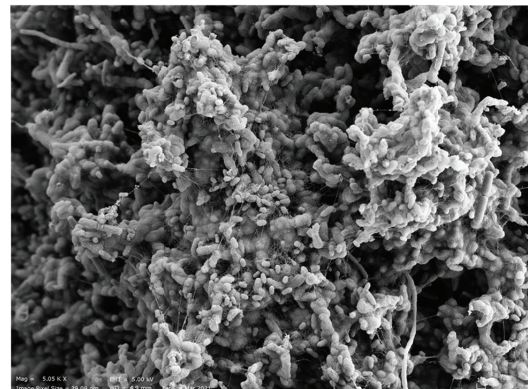


Figure 4.19 Scanning electron microscopy analysis of regiospecific organizational states of Salmonella biofilms at the air-liquid interface

SEM analysis provided us unprecedented information about the biofilm's different surface features and helped us perform regio-specific morphological analysis through the surface-bound biofilm, as shown in 4.19. However, the SEM intrinsically does not reveal the compositional distribution of the biofilm matrix. At lower magnifications, the bacterial structure seems densely packed structure as seen in 4.19a,b, but with the higher magnifications, those densely packed structures become porous and fibrous connections of extracellular matrix seen more clearly in Figure 4.20.

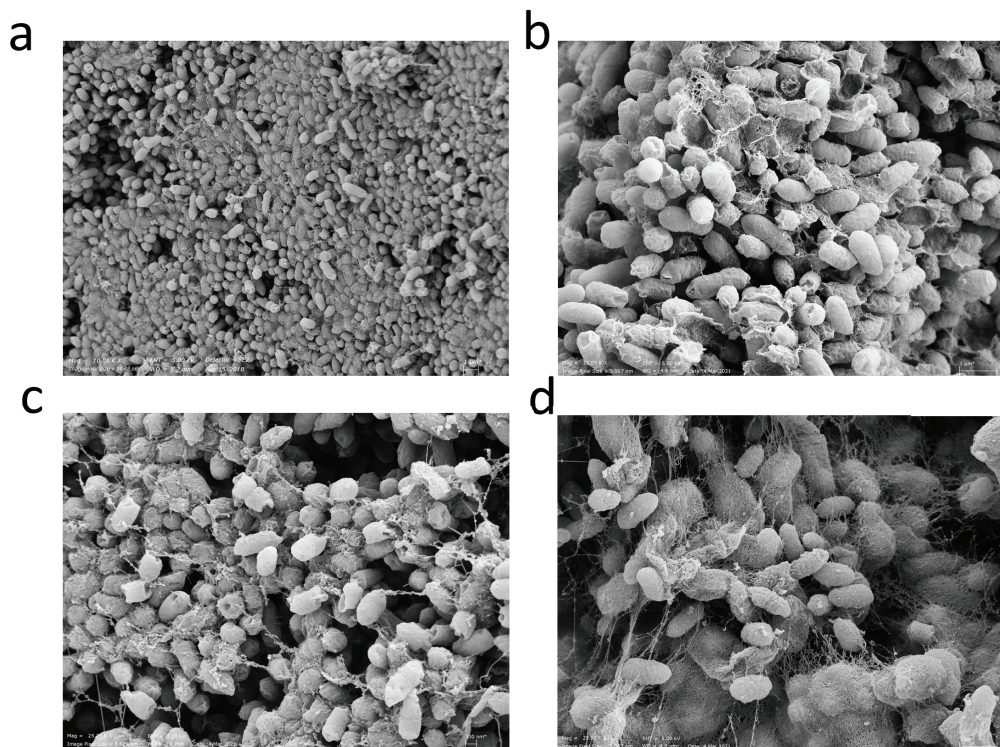


Figure 4.20 Scanning electron microscopy analysis of regiospecific organizational states of Salmonella biofilms at the air-liquid interface

CHAPTER 5

CONCLUSIONS

In the thesis, in situ monitoring biofilm formation to understand electrodynamics of the formation was proposed with a wild type and mutant strain at the air-liquid interface and in the bulk solution. The experiments were carried out with a BDD electrode, which allowed working at higher potentials and lower frequencies. The SWV experiments show that the biofilm formation at the air-liquid interface has new redox dynamics, and EIS revealed the resistive and capacitive effects of biofilm formation with time-dependent equivalent circuit fitting. As biofilm formation begins with cell growth and multiplication, changes in the first 12-20h can be dedicated to these steps. After 20h, the process has two mechanisms: the dispersion of the bacteria and the extracellular matrix formation. The capacitance and resistance of the extracellular matrix were taken into account with the new equivalent circuit model.

To illuminate the biofilm morphology of the biofilm, scanning electron microscopy were carried out. As seen in the images, ECM components connect the cells, while the biofilm also has a porous structure with dispersed cells. I believe that this method is beneficial for the monitoring of bacterial biofilm and for eukaryotic cells or other time-dependent mechanisms.

REFERENCES

- (1) Parlak, O.; Richter-Dahlfors, A. Bacterial Sensing and Biofilm Monitoring for Infection Diagnostics. *Macromolecular Bioscience*. 2020.
- (2) Flemming, H. C.; Wingender, J. The Biofilm Matrix. *Nature Reviews Microbiology*. 2010, pp 623–633.
- (3) Rumbaugh, K. P.; Sauer, K. Biofilm Dispersion. *Nat. Rev. Microbiol.*
- (4) Watnick, P.; Kolter, R. Biofilm, City of Microbes. *Journal of Bacteriology*. May 2000, pp 2675–2679.
- (5) Singh, R.; Paul, D.; Jain, R. K. Biofilms: Implications in Bioremediation. *Trends in Microbiology*. Elsevier Current Trends September 1, 2006, pp 389–397.
- (6) Botyanszki, Z.; Tay, P. K. R.; Nguyen, P. Q.; Nussbaumer, M. G.; Joshi, N. S. Engineered Catalytic Biofilms: Site-Specific Enzyme Immobilization onto E. Coli Curli Nanofibers. *Biotechnol. Bioeng.* **2015**, *112* (10), 2016–2024.
- (7) Fernandes, R.; Luo, X.; Tsao, C. Y.; Payne, G. F.; Ghodssi, R.; Rubloff, G. W.; Bentley, W. E. Biological Nanofactories Facilitate Spatially Selective Capture and Manipulation of Quorum Sensing Bacteria in a BioMEMS Device. *Lab Chip* **2010**, *10* (9), 1128–1134.
- (8) Kimura, Z. I.; Chung, K. M.; Itoh, H.; Hiraishi, A.; Okabe, S. Raoultella Electrica Sp. Nov., Isolated from Anodic Biofilms of a Glucose-Fed Microbial Fuel Cell. *Int. J. Syst. Evol. Microbiol.* **2014**, *64* (PART 4), 1384–1388.
- (9) Nussbaumer, M. G.; Nguyen, P. Q.; Tay, P. K. R.; Naydich, A.; Hysi, E.; Botyanszki, Z.; Joshi, N. S. Bootstrapped Biocatalysis: Biofilm-Derived Materials as Reversibly Functionalizable Multienzyme Surfaces. *ChemCatChem* **2017**, *9* (23), 4328–4333.
- (10) Castillo-Juárez, I.; Maeda, T.; Mandujano-Tinoco, E. A.; Tomás, M.; Pérez-Eretza, B.; García-Contreras, S. J.; Wood, T. K.; García-Contreras, R. Role of Quorum Sensing in Bacterial Infections. *World J. Clin. Cases* **2015**, *3* (7), 575.
- (11) Persat, A.; Nadell, C. D.; Kim, M. K.; Ingremeau, F.; Siryaporn, A.; Drescher, K.; Wingreen, N. S.; Bassler, B. L.; Gitai, Z.; Stone, H. A. The Mechanical World of Bacteria. *Cell*. 2015, pp 988–997.
- (12) Costerton, A. J. W.; Stewart, P. S.; Greenberg, E. P. Bacterial Biofilms : Persistent Common Cause Of. *Science (80-.)*. **2011**, *284* (5418), 1318–1322.

- (13) Richards, J. J.; Melander, C. Controlling Bacterial Biofilms. *ChemBioChem*. 2009, pp 2287–2294.
- (14) Desai, N.; Ardekani, A. M. Biofilms at Interfaces: Microbial Distribution in Floating Films. *Soft Matter* **2020**, *16* (7), 1731–1750.
- (15) Xu, Y.; Dhaouadi, Y.; Stoodley, P.; Ren, D. Sensing the Unreachable: Challenges and Opportunities in Biofilm Detection. *Curr. Opin. Biotechnol.* **2020**, *64*, 79–84.
- (16) Henrici, A. T. *Studies of Freshwater Bacteria: I. A Direct Microscopic Technique.*; 1933; Vol. 25.
- (17) Hoiby, N.; Olling, S. Pseudomonas Aeruginosa Infection in Cystic Fibrosis. Bacterial Effect of Serum from Normal Individuals and Patients with Cystic Fibrosis on P. Aeruginosa Strains from Patients with Cystic Fibrosis or Other Diseases. *Acta Pathol. Microbiol. Scand. - Sect. C Immunol.* **1977**, *85* (2), 107–114.
- (18) Costerton, J. W.; Geesey, G. G.; Cheng, K. J. How Bacteria Stick. *Sci. Am.* **1978**, *238* (1), 86–95.
- (19) Costerton, J. W.; Stewart, P. S.; Greenberg, E. P. Bacterial Biofilms: A Common Cause of Persistent Infections. *Science*. 1999, pp 1318–1322.
- (20) Hall-Stoodley, L.; Costerton, J. W.; Stoodley, P. Bacterial Biofilms: From the Natural Environment to Infectious Diseases. *Nature Reviews Microbiology*. 2004, pp 95–108.
- (21) Rumbaugh, K. P.; Sauer, K. Biofilm Dispersion. *Nature Reviews Microbiology*. 2020.
- (22) Götz, F. Staphylococcus and Biofilms. *Molecular Microbiology*. 2002, pp 1367–1378.
- (23) van der Kooij, D.; Veenendaal, H. R.; Baars-Lorist, C.; van der Klift, D. W.; Drost, Y. C. Biofilm Formation on Surfaces of Glass and Teflon Exposed to Treated Water. *Water Res.* **1995**.
- (24) Tauxe, R. V. Emerging Foodborne Pathogens. *Int. J. Food Microbiol.* **2002**, *78* (1–2), 31–41.
- (25) Scallan, E.; Hoekstra, R. M.; Angulo, F. J.; Tauxe, R. V.; Widdowson, M. A.; Roy, S. L.; Jones, J. L.; Griffin, P. M. Foodborne Illness Acquired in the United States—Major Pathogens. *Emerg. Infect. Dis.* **2011**, *17* (1), 7–15.
- (26) World Health Organization[WHO]. *GLOBAL HEALTH SECTOR STRATEGY ON SEXUALLY TRANSMITTED INFECTIONS 2016–2021 TOWARDS ENDING*

STIs; 2021; Vol. 68.

- (27) Wi, T.; Lahra, M. M.; Ndowa, F.; Bala, M.; Dillon, J. A. R.; Ramon-Pardo, P.; Eremin, S. R.; Bolan, G.; Unemo, M. Antimicrobial Resistance in *Neisseria Gonorrhoeae*: Global Surveillance and a Call for International Collaborative Action. *PLoS Med.* **2017**, *14* (7), e1002344.
- (28) Furst, A. L.; Francis, M. B. Impedance-Based Detection of Bacteria. *Chem. Rev.* **2019**, *119* (1), 700–726.
- (29) Høiby, N.; Bjarnsholt, T.; Moser, C.; Bassi, G. L.; Coenye, T.; Donelli, G.; Hall-Stoodley, L.; Holá, V.; Imbert, C.; Kirketerp-Møller, K.; Lebeaux, D.; Oliver, A.; Ullmann, A. J.; Williams, C.; ESCMID Study Group for Biofilms (ESGB); Consulting External Expert Werner Zimmerli. ESCMID* Guideline for the Diagnosis and Treatment of Biofilm Infections 2014. *Clin. Microbiol. Infect.* **2015**, *21* (S1), S1–S25.
- (30) Hall-Stoodley, L.; Stoodley, P.; Kathju, S.; Høiby, N.; Moser, C.; William Costerton, J.; Moter, A.; Bjarnsholt, T. Towards Diagnostic Guidelines for Biofilm-Associated Infections. *FEMS Immunol. Med. Microbiol.* **2012**, *65* (2), 127–145.
- (31) Li, C.; Renz, N.; Trampuz, A. Management of Periprosthetic Joint Infection. *Hip Pelvis* **2018**, *30* (3), 138.
- (32) Omar, A.; Wright, J.; Schultz, G.; Burrell, R.; Nadworny, P. Microbial Biofilms and Chronic Wounds. *Microorganisms* **2017**, *5* (1), 9.
- (33) Arciola, C. R.; Collamati, S.; Donati, E.; Montanaro, L. A Rapid PCR Method for the Detection of Slime-Producing Strains of *Staphylococcus Epidermidis* and *S. Aureus* in Periprostheses Infections. *Diagnostic Mol. Pathol.* **2001**, *10* (2), 130–137.
- (34) Vidal, M.; Kruger, E.; Durán, C.; Lagos, R.; Levine, M.; Prado, V.; Toro, C.; Vidal, R. Single Multiplex PCR Assay to Identify Simultaneously the Six Categories of Diarrheagenic *Escherichia Coli* Associated with Enteric Infections. *J. Clin. Microbiol.* **2005**, *43* (10), 5362–5365.
- (35) Cangelosi, G. A.; Meschke, J. S. Dead or Alive: Molecular Assessment of Microbial Viability. *Applied and Environmental Microbiology*. American Society for Microbiology 2014, pp 5884–5891.
- (36) Bej, A. K.; Mahbubani, M. H.; Atlas, R. M. Detection of Viable *Legionella Pneumophila* in Water by Polymerase Chain Reaction and Gene Probe Methods.

Appl. Environ. Microbiol. **1991**, *57* (2), 597–600.

- (37) Nilsson, K. P. R.; Herland, A.; Hammarström, P.; Inganäs, O. Conjugated Polyelectrolytes: Conformation-Sensitive Optical Probes for Detection of Amyloid Fibril Formation. *Biochemistry* **2005**, *44* (10), 3718–3724.
- (38) Choong, F. X.; Bäck, M.; Steiner, S. E.; Melican, K.; Nilsson, K. P. R.; Edlund, U.; Richter-Dahlfors, A. Nondestructive, Real-Time Determination and Visualization of Cellulose, Hemicellulose and Lignin by Luminescent Oligothiophenes. *Sci. Rep.* **2016**, *6* (1), 1–12.
- (39) Klingstedt, T.; Nilsson, K. P. R. Luminescent Conjugated Poly- and Oligothiophenes: Optical Ligands for Spectral Assignment of a Plethora of Protein Aggregates. In *Biochemical Society Transactions*; 2012; Vol. 40, pp 704–710.
- (40) Klingstedt, T.; Blechschmidt, C.; Nogalska, A.; Prokop, S.; Häggqvist, B.; Danielsson, O.; Engel, W. K.; Askanas, V.; Heppner, F. L.; Nilsson, K. P. R. Luminescent Conjugated Oligothiophenes for Sensitive Fluorescent Assignment of Protein Inclusion Bodies. *ChemBioChem* **2013**, *14* (5), 607–616.
- (41) Åslund, A.; Sigurdson, C. J.; Klingstedt, T.; Grathwohl, S.; Bolmont, T.; Dickstein, D. L.; Glimsdal, E.; Prokop, S.; Lindgren, M.; Konradsson, P.; Holtzman, D. M.; Hof, P. R.; Heppner, F. L.; Gandy, S.; Jucker, M.; Aguzzi, A.; Hammarström, P.; Nilsson, K. P. R. Novel Pentameric Thiophene Derivatives for in Vitro and in Vivo Optical Imaging of a Plethora of Protein Aggregates in Cerebral Amyloidoses. *ACS Chem. Biol.* **2009**, *4* (8), 673–684.
- (42) Klingstedt, T.; Åslund, A.; Simon, R. A.; Johansson, L. B. G.; Mason, J. J.; Nyström, S.; Hammarström, P.; Nilsson, K. P. R. Synthesis of a Library of Oligothiophenes and Their Utilization as Fluorescent Ligands for Spectral Assignment of Protein Aggregates. *Org. Biomol. Chem.* **2011**, *9* (24), 8356–8370.
- (43) Choong, F. X.; Bäck, M.; Fahlén, S.; Johansson, L. B. G.; Melican, K.; Rhen, M.; Nilsson, K. P. R.; Richter-Dahlfors, A. Real-Time Optotracing of Curli and Cellulose in Live Salmonella Biofilms Using Luminescent Oligothiophenes. *npj Biofilms Microbiomes* **2016**, *2* (May), 1–11.
- (44) Choong, F. X.; Bäck, M.; Fahlén, S.; Johansson, L. B. G.; Melican, K.; Rhen, M.; Nilsson, K. P. R.; Richter-Dahlfors, A. Real-Time Optotracing of Curli and Cellulose in Live Salmonella Biofilms Using Luminescent Oligothiophenes. *npj Biofilms Microbiomes* **2016**, *2* (1), 1–11.
- (45) Ronkainen, N. J.; Halsall, H. B.; Heineman, W. R. Electrochemical Biosensors.

- Chem. Soc. Rev.* **2010**, 39 (5), 1747–1763.
- (46) Monzó, J.; Insua, I.; Fernandez-Trillo, F.; Rodriguez, P. Fundamentals, Achievements and Challenges in the Electrochemical Sensing of Pathogens. *Analyst* **2015**, 140 (21), 7116–7128.
- (47) Gouy, M. Sur La Constitution de La Charge Électrique à La Surface d'un Électrolyte. *J. Phys. Theor. Appl* **1910**, 9 (1).
- (48) Chapman, D. L. LI. A Contribution to the Theory of Electrocapillarity . *London, Edinburgh, Dublin Philos. Mag. J. Sci.* **1913**, 25 (148), 475–481.
- (49) Teng, Z.; Kuang, X.; Wang, J.; Zhang, X. Real-Time Cell Analysis - A New Method for Dynamic, Quantitative Measurement of Infectious Viruses and Antiserum Neutralizing Activity. *J. Virol. Methods* **2013**, 193 (2), 364–370.
- (50) Golke, A.; Cymerys, J.; Słońska, A.; Dzieciatkowski, T.; Chmielewska, A.; Tucholska, A.; Bańbura, M. W. The XCELLigence System for Real-Time and Label-Free Analysis of Neuronal and Dermal Cell Response to Equine Herpesvirus Type 1 Infection. *Pol. J. Vet. Sci.* **2012**, 15 (1), 151–153.
- (51) Giaever, I.; Keese, C. R. Electric Cell-Substrate Impedance Sensing Concept to Commercialization. *Cancer Metastasis - Biol. Treat.* **2012**, 17 (1), 1–19.
- (52) Wegener, J.; Keese, C. R.; Giaever, I. Electric Cell-Substrate Impedance Sensing (ECIS) as a Noninvasive Means to Monitor the Kinetics of Cell Spreading to Artificial Surfaces. *Exp. Cell Res.* **2000**, 259 (1), 158–166.
- (53) Vadhva, P.; Hu, J.; Johnson, M. J.; Stocker, R.; Braglia, M.; Brett, D. J. L.; Rettie, A. J. E. Electrochemical Impedance Spectroscopy for All-Solid-State Batteries: Theory, Methods and Future Outlook. *ChemElectroChem*. John Wiley and Sons Inc June 1, 2021, pp 1930–1947.
- (54) Muñoz-Berbel, X.; Vigués, N.; Mas, J.; Jenkins, A. T. A.; Muñoz, F. J. Impedimetric Characterization of the Changes Produced in the Electrode-Solution Interface by Bacterial Attachment. *Electrochem. commun.* **2007**, 9 (11), 2654–2660.
- (55) Lvovich, V. F. Equivalent-Circuit Elements and Modeling of the Impedance Phenomenon. In *Impedance Spectroscopy*; John Wiley & Sons, Inc.: Hoboken, NJ, USA, 2012; pp 37–47.
- (56) Ciucci, F. Modeling Electrochemical Impedance Spectroscopy. *Current Opinion in Electrochemistry*. Elsevier B.V. February 1, 2019, pp 132–139.
- (57) Stupin, D. D.; Kuzina, E. A.; Abelit, A. A.; Emelyanov, A. K.; Nikolaev, D. M.;

- Ryazantsev, M. N.; Koniakhin, S. V.; Dubina, M. V. Bioimpedance Spectroscopy: Basics and Applications. *ACS Biomater. Sci. Eng.* **2021**, 7 (6), 1962–1986.
- (58) Ben-Yoav, H.; Freeman, A.; Sternheim, M.; Shacham-Diamand, Y. An Electrochemical Impedance Model for Integrated Bacterial Biofilms. In *Electrochimica Acta*; 2011; Vol. 56, pp 7780–7786.
- (59) Bisquert, J.; Compte, A. Theory of the Electrochemical Impedance of Anomalous Diffusion. *J. Electroanal. Chem.* **2001**, 499 (1), 112–120.
- (60) Liu, L.; Xu, Y.; Cui, F.; Xia, Y.; Chen, L.; Mou, X.; Lv, J. Monitoring of Bacteria Biofilms Forming Process by In-Situ Impedimetric Biosensor Chip. *Biosens. Bioelectron.* **2018**, 112, 86–92.
- (61) Song, J.; Li, Y.; Yin, F.; Zhang, Z.; Ke, D.; Wang, D.; Yuan, Q.; Zhang, X.-E. Enhanced Electrochemical Impedance Spectroscopy Analysis of Microbial Biofilms on an Electrochemically In Situ Generated Graphene Interface. *ACS Sensors* **2020**, 5 (6), 1795–1803.
- (62) Amblard, M.; Fehrentz, J. A.; Martinez, J.; Subra, G. Fundamentals of Modern Peptide Synthesis. *Methods Mol. Biol.* **2005**, 298, 3–24.